E-Cigarette Exposure in Zebrafish Leads to Defects in Neurogenesis Similar to Those Found Following Exposure to Traditional Tobacco Cigarettes

Sicheng Lee[†1], Sam Shang[†1], Shen Yen Tsou[†1], Rami Halabi[2], Patrick Ciechanski[2], Deirdre Lobb[3], Cairine Logan[1*]

[†]Authors contributed equally to the data collection and manuscript preparation.

[1]Department of Cell Biology and Anatomy, Department of Biochemistry and Molecular Biology, Alberta Children's Hospital Research Institute, Cumming School of Medicine, 3330 Hospital Drive NW, Calgary, Alberta, Canada, T2N 4N1.

[2]Department of Neuroscience, Hotchkiss Brain Institute, University of Calgary, 3330 Hospital Drive NW, Calgary, Alberta, Canada, T2N 4N1.

[3]O'Brien Centre for the Bachelor of Health Sciences Program, University of Calgary, 3330 Hospital Drive NW, Calgary, Alberta, Canada, T2N 4N1.

ABSTRACT

Nicotine has been shown to have neuroteratogenic effects on the developing fetus. In recent years, nicotine-containing electronic cigarettes (e-cigarettes) have become a popular alternative to traditional tobacco cigarettes, especially among pregnant women who may believe that e-cigarettes are comparably less harmful. The health effects of e-cigarette smoke exposure during prenatal life, however, are currently not well known. This study compared the neuroteratogenic effects of embryonic exposure to nicotine-containing e-cigarette smoke condensate (e-CSC) and cigarette smoke condensate (CSC) on retinal ganglion cell (RGC) development in a zebrafish (Danio rerio) model. Embryos of the transgenic zebrafish, Tg(-17.6 is l2b:GFP)^{zc7}, were dechorionated at 24 hours post-fertilization (hpf) and exposed to varying concentrations of e-CSC or CSC for 46 hours. The number of surviving embryos was counted at 72 hpf. The median lethal dose (LD$_{50}$) for CSC and e-CSC was calculated from the proportion of non-surviving fish to the total number of fish exposed. Fluorescent images were subsequently taken of all surviving embryos and used to measure gross eye size and differentiated RGC layer size along the dorsal-ventral and nasal-temporal axes, and to measure width of the optic nerve. The LD$_{50}$ of e-CSC was determined at 5.06x, compared to an LD$_{50}$ of CSC at 0.035x. Exposure to both e-CSC and CSC resulted in significant reductions in gross eye size and optic nerve width. While e-cigarettes were comparably less toxic than cigarettes, the similar morphological eye changes and RGC developmental perturbations observed following exposure to e-CSC and CSC suggest that nicotine containing e-cigarettes are as harmful to developing neurons as cigarettes.

KEYWORDS

electronic cigarettes, zebrafish, neurogenesis, retinal ganglion cells, *Tg(-17.6isl2b:GFP)^{zc7}*
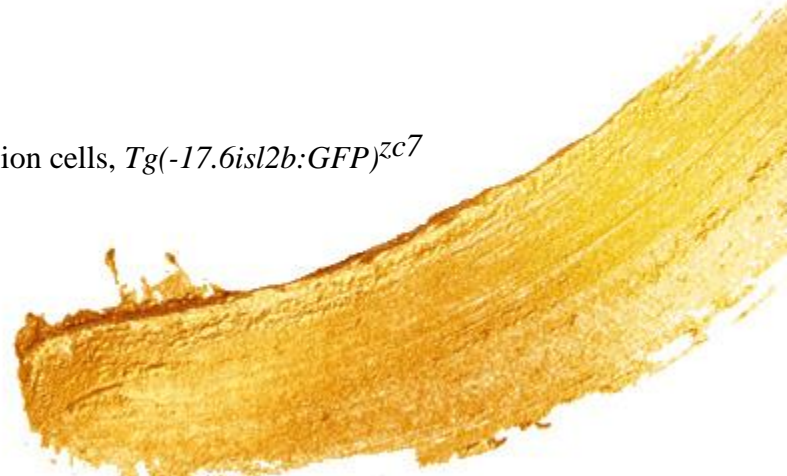
INTRODUCTION

Despite the well-documented adverse effects of nicotine on fetal health, there has been little decline in the use of traditional tobacco cigarettes during pregnancy over the past decade with between 10-14% of women continuing to smoke while pregnant (Alshaarawy & Anthony, 2015; England *et al.*, 2017; Kurti *et al.*, 2017). Prevalence of electronic cigarette (e-cigarette) use during pregnancy, on the other hand, has been steadily rising since their introduction to the North American market in 2007. Indeed, a recent 2015 cross-sectional survey of 382 pregnant women receiving care at a university-based obstetrical clinic in the United States (US) found that an increasing number of women (i.e. approximately 12%) were users of such electronic nicotine delivery systems (ENDS) (Bhandari *et al.*, 2018; Kurti *et al.*, 2017). Data from a subset of pregnant women (N=388) in a slightly earlier (i.e. 2013-14) longitudinal cohort study of youth and adults in the US non-institutionalized population (i.e. drawn from the Public Use File of the Population Assessment of Tobacco and Health Study), reported only 5% ENDS users (Bhandari *et al.*, 2018; Kurti *et al.*, 2017). In addition, 28-30% of pregnant women in these studies reported dual usage of both ENDS and tobacco cigarettes (Bhandari *et al.*, 2018; Kurti *et al.*, 2017). The common perception among pregnant women of e-cigarettes as a safer alternative to traditional tobacco cigarettes as well as their widespread marketing as a smoking cessation tool has likely contributed to their increasing use in this population (Bhandari *et al.*, 2018; Wagner, Camerota, & Propper, 2017). Little, however, is known about the potential impact of nicotine containing e-cigarettes on pre- and post-embryonic development of the fetus. Indeed, no randomized clinical trials have been conducted to date on the use of e-cigarettes during pregnancy (van der Eijk, Petersen, & Bialous, 2017). There are also very few published studies using animal models of the developmental outcomes of nicotine exposure from e-cigarettes (Chen *et al.*, 2018; Kennedy, Kandalam, Olivares-Navarrete, & Dickinson, 2017; Palpant, Hofsteen, Pabon, Reinecke, & Murry, 2015).

The neuroteratogenic effects of nicotine on developing embryos are, however, well established (England *et al.*, 2017). Nicotine is known to cross the placental barrier and accumulates in the fetus at levels similar to or higher than in the mother (Jordanov, 1990; Köhler, Avenarius, Rabsilber, Gerloff, & Jorch, 2010). Nicotine is known to interact with nicotinic acetylcholine receptors (nAChRs), critical signal transducers for neuronal proliferation and differentiation in the developing fetal brain (Poorthuis, Goriounova, Couey, & Mansvelder, 2009). Prenatal nicotine exposure has been shown to disrupt normal neurogenesis and can lead to premature neuronal differentiation, abnormal neuronal migration, outgrowth, synaptogenesis and increased apoptosis (Berger, Gage, & Vijayaraghavan, 1998; Roy, Seidler, & Slotkin, 2002; Slotkin *et al.*, 2015; Slotkin *et al.*, 2017; Wang, Wang, Zhu, & Qin, 2018). Prenatal nicotine exposure has also been associated with long lasting neurobehavioural deficits in resulting offspring (Alkam *et al.*, 2017; Hamer, Ford, Stamatakis, Dockray, & Batty, 2011; Law *et al.*, 2003; Pagani, 2014; Yolton *et al.*, 2009; Zhu *et al.*, 2017).

This study aimed to investigate the overall toxicity and neuroteratogenic effect of prenatal exposure to nicotine containing e-cigarettes directly *in vivo* using zebrafish as a model system. Specifically, we used the developing visual system to compare morphological consequence of exposure to nicotine containing e-cigarette smoke condensate (e-CSC) and tobacco cigarette smoke condensate (CSC) on

development of retinal ganglion cells (RGCs) as well as assess and compare whole embryo viability following chronic exposure.

MATERIALS AND METHODS

Animals

Transgenic *Tg(-17.6isl2b:GFP)^{zc7}* zebrafish (*Danio rerio*) that express green fluorescent protein driven by the *Islet-1 2b* promoter/enhancer (Pittman, Law, & Chien, 2008), were kindly provided by Dr. Sarah McFarlane (University of Calgary, Calgary, AB). Adult fish were maintained at 28.5°C and bred essentially as described in Westerfield (Westerfield, 2007). Embryos were collected within 30 min after fertilization and were allowed to develop in uncrowded conditions in zebrafish embryo medium (E3) for 24 hours (hrs) at 28°C. All animal procedures were approved by the University of Calgary Animal Care Committee.

Cigarette and e-Cigarette Smoke Condensate

3R4F research grade cigarettes (University of Kentucky, Lexington, KY, USA) containing an average of 0.726 mg nicotine per cigarette were used to create CSC via a previously described syringe apparatus (Hudy, Traves, Wiehler, & Proud, 2010). Briefly, the apparatus was primed with one full cigarette prior to condensate synthesis. Cigarette smoke from one cigarette was then bubbled into 4ml E3 containing 0.0003% 1-phenyl-2-thiourea (PTU; Sigma, St. Louis, MO) at a rate of approximately five min per cigarette. The resulting solution was filtered with 0.22 μm pore filter (Pall (Canada) Ltd., Mississauga, ON) and standardized via Nanodrop photospectroscopy reading at 320 nm. This solution was considered to be 1x.

To create 1x e-CSC, a Kanger Top™ Evod E-Cigarette Atomizer (KangerTech, Shenzhen GuangDong, China) was used to vape B&H tobacco E-juice (Cool Vape, Calgary, AB)

containing 6 mg/ml nicotine as above via a separate syringe apparatus. The apparatus was similarly primed using approximately 121 □l of E-juice (i.e. volume equals nicotine equivalent of one research grade cigarette) prior to condensate synthesis. Approximately 121 □l E-juice was then bubbled as above into 4 ml E3 containing 0.0003% PTU (Sigma, St. Louis, MO). The same atomizer and syringe apparatus was also subsequently used to vape B&H tobacco E-juice (Cool Vape, Calgary, AB) containing 24 mg/ml nicotine to produce a more concentrated 10x e-CSC. The apparatus was similarly primed using 30.25 □l of E-juice (i.e. volume equals nicotine equivalent of one research grade cigarettes) prior to bubbling 302.5 □l of E-juice (i.e. volume equals nicotine equivalent of ten research grade cigarettes) as above into 4 ml E3 containing 0.0003% PTU (Sigma, St. Louis, MO) and standardized via Nanodrop photospectroscopy reading at 320 nm. CSC and e-CSC was prepared the day before use and stored at -20°C until needed.

Condensate Treatment

Embryos were manually dechorionated at 24 hpf and ten embryos transferred to a single well of a 24-well tissue culture dish (Corning Incorporated (USA), Corning, NY) for subsequent treatment with either CSC or e-CSC. At 26 hpf, embryos were exposed to various dilutions of 1x CSC, 1x e-CSC or 10x e-CSC in E3 containing 0.0003% PTU and incubated at 28°C for 46 hrs. PTU was included during treatment (i.e. from 26 to 72 hpf) to reduce pigmentation. E3 containing 0.0003% PTU (i.e. vehicle alone) served as a negative control. Dead fish were removed at 4, 20, 28 and 44 hours post treatment.

LD$_{50}$ Value Determination

At 72 hpf, the number of live fish were counted and the proportions of dead fish to the total number of exposed embryos were used to generate median lethal dose (LD$_{50}$)

curves via GraphPad Prism7 (GraphPad Software, Inc., La Jolla, CA). Three to six independent experiments at each of the concentrations tested were used to determine the LD_{50} for CSC while five independent experiments at each of the concentrations tested were used to determine the LD_{50} for e-CSC.

Fluorescence Imaging

All surviving embryos from the aforementioned protocol were fixed at 72 hpf in 4% paraformaldehyde (PFA; Sigma, St Louis, MO) in phosphate-buffered saline (PBS; 140 mM NaCl, 10 mM phosphate buffer, and 3 mM KCl, pH 7.4) for 25 min, washed with PBS for 10 min, and suspended in 500 µl PBS prior to transferring to an embossed sylgard (Corning Incorporated (USA), Corning, NY) plate for photography. Non-fluorescent fish (approximately 1/3) were excluded from the sample. Imaging was performed with Zeiss Lumar V12 microscope (Carl Zeiss, Inc., Thornwood, NY) equipped with Zeiss AxioCam (Carl Zeiss, Inc., Thornwood, NY) and AxioVision 4.6 software (Carl Zeiss, Inc., Thornwood, NY) at 80x magnification.

Measuring and Statistics

AxioVision 4.6 software (Carl Zeiss, Inc., Thornwood, NY) was used to obtain blinded measurements of gross eye and differentiated RGC layer size along the dorsal-ventral (DV) and nasal-temporal (NT) axes for the right eye, and the width of both the left and right optic nerves as they exited the eye. The RGC layer DV- and NT-axes lengths were standardized to the DV- and NT-axes lengths of the gross eye. Optic nerve width was standardized to the DV-axis length of the gross eye. A Student's t-test with p<0.05 was used to test for significant differences in gross eye size, standardized RGC size and average standardized optic nerve width between embryos treated with CSC or e-CSC and control embryos. Qualitative observations between groups were made of axon guidance and neuropil formation.

RESULTS

The LD_{50} value of cigarette and e-cigarette smoke condensate on zebrafish embryos

Exposure of zebrafish embryos to CSC or e-CSC resulted in a concentration dependent decrease in survival (**Figure. 1A and 1B**). The LD_{50} of CSC was determined at 0.035x (N=3-6) while the LD_{50} of e-CSC was determined at 5.06x (N=5). All embryos died within 20 hrs following exposure to 1x CSC. In contrast, there was limited embryo death (i.e. $7.08 \pm 1.65\%$; N=12, n=236) following exposure to E3 containing 0.0003% PTU (i.e. vehicle alone) during the course of the experiment (data not shown) or following exposure to 1x e-CSC (**Figure 1B**).

Similar behavioral and morphological malformations were observed following exposure to e-CSC or CSC. Embryos incubated in concentrations at or slightly below the LD_{50} for both e-CSC (i.e. 5x) and CSC (i.e. 0.025x) showed reduced or completely lost, spontaneous muscular twitching and voluntary movements compared to controls from 44-72 hpf. In addition, pericardial edema and a striking reduction in cranial size compared to controls were noted in both experimental groups (**Figure. 2B and 2C**). Embryo malformations were not deemed to be due to developmental delay as differentiation of the trigeminal ganglia and Rohon-Beard mechanosensory neurons were unperturbed in all experimental paradigms (**Figure. 2A-C**).

Condensate exposure reduces gross eye size

To quantify gross eye size, two parameters were used – dorsal/ventral length and nasal/temporal length. For each treatment group, respective controls were used to compare to limit clutch differences. Interestingly, eye size was significantly

reduced in embryos exposed to concentrations at or slightly below the LD_{50} of CSC (0.025x; **Figure. 2D**) and e-CSC (5x; **Figure. 2E**). In CSC embryos, dorsal/ventral length (N=2, n=23; p<0.05) and nasal/temporal length (N=2, n=23; p<0.05) were significantly reduced 5.6% or 6.5%

respectively compared to controls (N=2, n=16). Similarly, e-CSC incubated embryos showed a significant reduction of 15.7% and 17.2% in the dorsal/ventral (N=2, n=25; p<0.0001) and nasal/temporal (N=2, n=25; p<0.0001) axes respectively compared to controls (N=2, n=14).
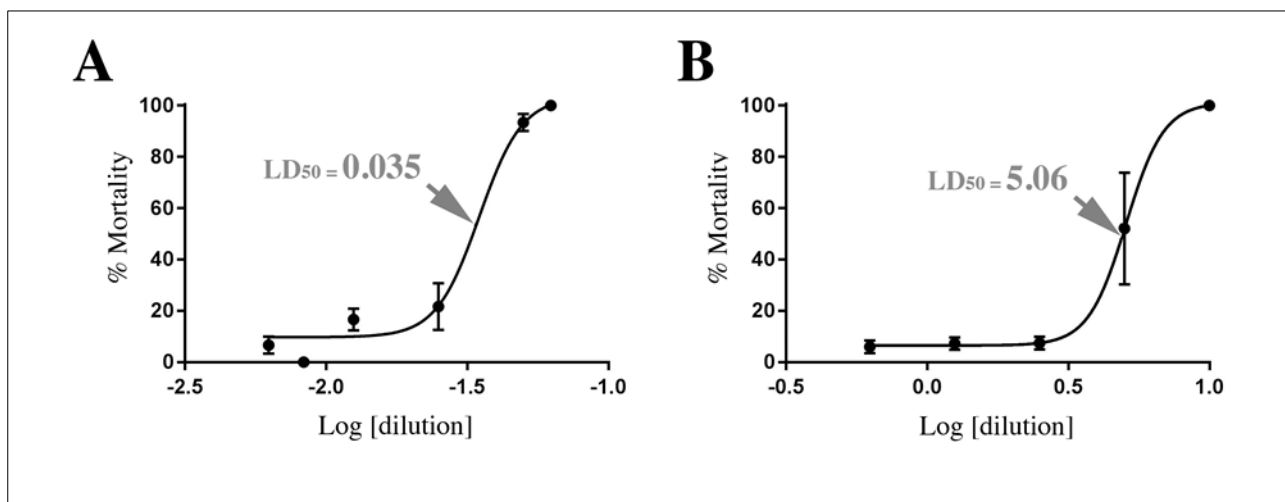

Figure 1. Dose-effect survival curves of chronic exposure to CSC (A) and e-CSC (B). The median lethal dose (LD_{50}) was determined at 72 hpf following a 46 hour exposure. The LD_{50} of CSC was 0.035x (N=3-6). The LD_{50} of e-CSC was 5.06x (N=5). Data represented as mean±SEM.

Retinal ganglion cell development is perturbed in condensate exposures

To determine the effects on RGC development, the *Tg(-17.6isl2b:GFP)^{zc7}* line was utilized. In this transgenic reporter, RGCs (as well as the trigeminal ganglia and Rohon-Beard mechanosensory neurons) are labeled by green fluorescent protein. RGCs are the only output neuron of the eye (Nawrocki, 1985) therefore, optic nerve measurements were made as a

proportional analysis of RGC number. Indeed, when normalized to eye width, the optic nerve was significantly thinner in the CSC (N=2, n=23; p<0.0001) and e-CSC (N=2, n=25; p<0.001) exposed embryos compared to controls (i.e. 23.3% and 24% respectively). In fact, RGC differentiation was perturbed in condensate exposed embryos, as evidenced by reduced reporter expression within the neural retina (**Figure. 2A-C and Figure. 2F-H**), and a substantial loss of neuropil of RGC axon terminals (**Figure. 2A-C**).
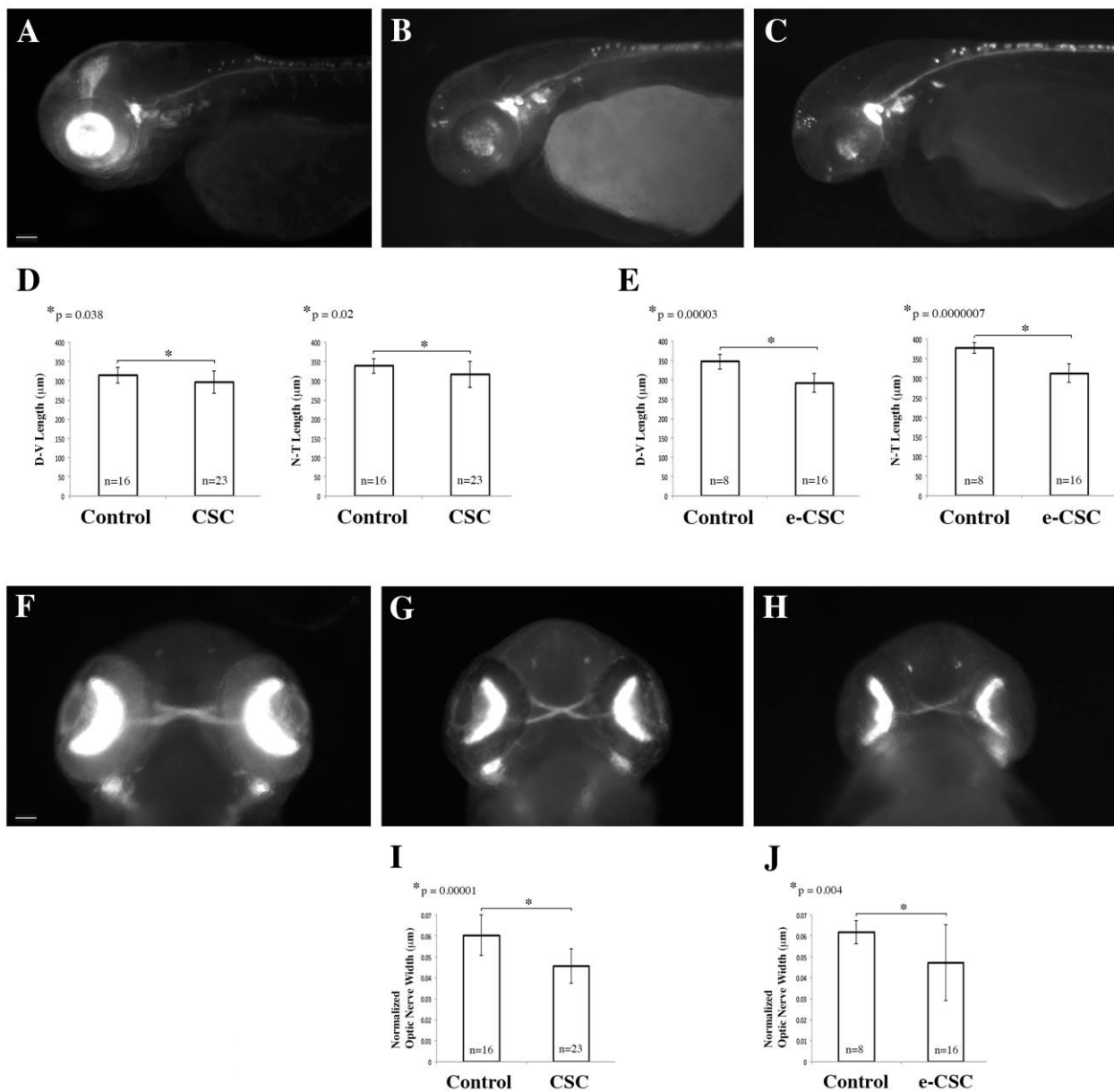
Figure 2. Defective RGC neurogenesis in treated embryos. Fluorescent images of lateral eye (A-C) and ventral optic nerve (F-H) at 72 hpf in *Tg(-17.6isl2b:GFP)*^{zc7} embryos treated with DMSO (A,F), CSC (B,G) or e-CSC (C,H). Quantification of eye size in dorso-ventral (D-V) and nasal-temporal (N-T) axis (D,E) of embryos. Quantification of optic nerve width (I,J) of embryos. Data represented as mean ± SEM. *p<0.05.

DISCUSSION

Given the increasing use of e-cigarettes among pregnant women, it is important to better understand the consequences of e-cigarette exposure on fetal health. Here we use the developing visual system of zebrafish as a model system to specifically determine the neurodevelopmental consequences of chronic prenatal exposure to nicotine containing e-CSC directly *in vivo*. Overall, e-CSC was found to be less toxic than CSC to the embryo as a whole when exposed at 26 hpf for 46 hrs. However, the morphological consequence of such exposure on gross size of the eye and development of retinal ganglion cells were identical. Gross eye size was significantly reduced along both the dorsal/ventral and nasal/temporal axis at 72 hpf compared to controls following exposure to either e-CSC or CSC at concentrations at or slightly lower than their respective LD_{50}. In addition, the number of RGCs present in the eye was significantly reduced at 72 hpf compared to controls following similar exposure as assessed quantitatively by the width of the optic nerve as well as qualitatively as a marked reduction of reporter expression with the neural retina and substantial loss of the neuropil of RGC axon terminals.

Consistent with our results, a recent study comparing the developmental effect of e-CSC and CSC on cardiac differentiation also showed that CSC was more toxic than e-CSC when zebrafish embryos were exposed at day 0 (i.e. early cleavage stages) for a slightly longer developmental period (i.e. 72 hrs) (Palpant *et al.*, 2015). Indeed, embryos exposed to CSC containing 34 $\square$M nicotine showed a significant decrease in survival at both 24 and 48 hours post exposure (hpe) compared to controls with no embryos surviving to 72 hpe while embryos exposed to e-CSC containing the same amount of nicotine only showed a significant decrease at 48 hpe when compared to controls and approximately 6% (as opposed to 0% of CSC exposed embryos) survived to 72 hpe.

Interestingly, zebrafish embryos similarly exposed to 1.25 or 2.5% 1,2-propanediol (also known as propylene glycol), the main component of e-cigarette liquid, had little to no effect on embryo survival compared to controls (Massarsky, Abdel, Glazer, Levin, & Di Giulio, 2018) suggesting that other components of e-CSC contribute to its toxicity.

Numerous *in vitro* studies using a wide variety of established and primary cell lines as well as stem cells have also previously shown that e-CSC was significantly less cytotoxic when compared to CSC (Anderson, Majeste, Hanus, & Wang, 2016; Anthérieu *et al.*, 2017; Azzopardi *et al.*, 2016; Cervellati *et al.*, 2014; Chun, Moazed, Calfee, Matthay, & Gotts, 2017; Farsalinos *et al.*, 2013; Otręba, Kośmider, Knysak, Warncke, & Sobczak, 2018; Putzhammer *et al.*, 2016; Romagna *et al.*, 2013; Scheffler, Dieken, Krischenowski, & Aufderheide, 2015; Singh, Luquet, Smith, Potgieter, & Ragazzon, 2016). However, the acute cytotoxicity of e-CSC has been shown to be highly variable and depends on the nature of the solution of e-liquid used to produce the condensate, the method of vaping, the ENDS battery voltage output as well as the sensitivity of cells employed in the assay (Kaur, Muthumalage, & Rahman, 2018). Indeed, some e-CSC showed cytotoxic effects *in vitro* that were similar to that of CSC while others displayed little to no cytotoxicity (Anthérieu *et al.*, 2017; Putzhammer *et al.*, 2016).

e-CSC is generally thought to contain fewer known toxic and carcinogenic compounds than CSC. Consistent with this, the levels of some of the most toxic and carcinogenic compounds found in CSC including various carbonyl compounds, volatile organic compounds, tobacco-specific nitrosamines and metals were previously shown to be up to 450-fold lower in e-CSC from tobacco flavored e-cigarette products similar to that tested herein, than in CSC from standard reference cigarettes (Goniewicz *et al.*, 2014). Notably, newer ENDS are manufactured using stainless steel to help minimize heavy metal exposure (Tegin, Mekala, Sarai, &

Lippmann, 2018). However, the vehicle (typically propylene glycol and glycerol) as well as specific flavorings used in various e-cigarette products may potentially contribute toxic and carcinogenic compounds to e-CSC that are not found in CSC such as hemiacetal, diacetyl, 2,3-pentanedione, and acetoin (Allen *et al.*, 2016; Jensen, Luo, Pankow, Strongin, & Peyton, 2015).

Most, but not all, e-cigarette liquids also contain varying levels of nicotine. Nicotine is known to be a neuroteratogen (England *et al.*, 2017). Numerous studies have shown that nicotine induces apoptosis in several neuronal cell types, including both primary and immortalized rat hippocampal progenitor cells, rat dentate gyrus neurons, murine olfactory bulb neurons and in RGCs (Berger *et al.*, 1998; Evereklioglu *et al.*, 2003; Jang *et al.*, 2002; Mechawar *et al.*, 2004; Roy *et al.*, 2002). Indeed, the number of RGCs in the retina of postnatal day 30 rat pups from mothers exposed on gestational day 9-21 to nicotine at plasma levels similar to those found in smokers, showed a 20.7% decrease compared to controls (Evereklioglu *et al.*, 2003). This compares favorably with the approximately 23 to 24% reduction we observed in the width of the optic nerve (i.e. indirect measure of RGC number) following exposure to CSC and e-CSC respectively at concentrations at or slightly lower than their LD_{50}.

The functional paralysis noted herein at 44 hpf was also previously observed following *in vivo* exposure from 22-72 hpf of zebrafish embryos to sub-lethal doses (i.e. approximately 15 or 30 ☐M) of nicotine (Menelaou, Paul, Perera, & Svoboda, 2015; Svoboda, Vijayaraghavan, & Tanguay, 2002; Welsh, Tanguay, & Svoboda, 2009). Indeed, nicotine was shown to directly affect development of both primary and secondary motoneurons resulting in delayed neurogenesis and axonal pathfinding errors following exposure. Such effects were found to be independent of nicotine induced muscle degeneration. Furthermore, activation of nAChRs has also previously been shown to directly regulate neurite outgrowth *in vitro* in several neuronal subtypes including chick ciliary ganglion and *Xenopus* spinal neurons (Pugh & Berg, 1994; Zheng, Felder, Connor, & Poo, 1994). The nicotine-induced activation of nAChRs *in vitro* led to inhibition of neurite extension and induced partial retraction of neurites in a calcium-dependent manner. Thus, the substantial loss of the neuropil of RGC axon terminals in the optic tectum observed herein is likely due to a combination of neuronal cell loss and neurite retraction and/or axonal pathfinding defects in the remaining RGC.

CONCLUSIONS

Prevalence of e-cigarette use among pregnant women continues to increase while studies regarding their safety remain inconclusive. Little, however, is known about the short and long-term developmental consequences of exposure to e-cigarettes *in utero* on the fetus. Here we used zebrafish as a model system to compare the toxicity and neuroteratogenic effects of nicotine containing e-CSC and CSC directly *in vivo*. We showed that although e-CSC was found overall to be less toxic to the embryo than CSC, the developmental consequences on RGC neurogenesis were identical. Our results highlight a critical need for healthcare providers to promote awareness of the potential adverse health risks of ENDS use in pregnant women and for appropriate regulatory policies to be developed specific to this population.

ACKNOWLEDGEMENTS

References

1. Alkam, T., Mamiya, T., Kimura, N., Yoshida, A., Kihara, D., Tsunoda, Y., . . . Nabeshima, T. (2017). Prenatal nicotine exposure decreases the release of dopamine in the medial frontal cortex and induces atomoxetine-responsive neurobehavioral deficits in mice. Psychopharmacology (Berl), 234(12), 1853-1869. doi:10.1007/s00213-017-4591-z

2. Allen, J. G., Flanigan, S. S., LeBlanc, M., Vallarino, J., MacNaughton, P., Stewart, J. H., & Christiani, D. C. (2016). Flavoring Chemicals in E-Cigarettes: Diacetyl, 2,3-Pentanedione, and Acetoin in a Sample of 51 Products, Including Fruit-, Candy-, and Cocktail-Flavored E-Cigarettes. Environ Health Perspect, 124(6), 733-739. doi:10.1289/ehp.1510185

3. Alshaarawy, O., & Anthony, J. C. (2015). Month-wise estimates of tobacco smoking during pregnancy for the United States, 2002-2009. Matern Child Health J, 19(5), 1010-1015. doi:10.1007/s10995-014-1599-4

4. Anderson, C., Majeste, A., Hanus, J., & Wang, S. (2016). E-Cigarette Aerosol Exposure Induces Reactive Oxygen Species, DNA Damage, and Cell Death in Vascular Endothelial Cells. Toxicol Sci, 154(2), 332-340. doi:10.1093/toxsci/kfw166

5. Anthérieu, S., Garat, A., Beauval, N., Soyez, M., Allorge, D., Garçon, G., & Lo-Guidice, J. M. (2017). Comparison of cellular and transcriptomic effects between electronic cigarette vapor and cigarette smoke in human bronchial epithelial cells. Toxicol In Vitro, 45(Pt 3), 417-425. doi:10.1016/j.tiv.2016.12.015

6. Azzopardi, D., Patel, K., Jaunky, T., Santopietro, S., Camacho, O. M., McAughey, J., & Gaça, M. (2016). Electronic cigarette aerosol induces significantly less cytotoxicity than tobacco smoke. Toxicol Mech Methods, 26(6), 477-491. doi:10.1080/15376516.2016.1217112

7. Berger, F., Gage, F. H., & Vijayaraghavan, S. (1998). Nicotinic receptor-induced apoptotic cell death of hippocampal progenitor cells. J Neurosci, 18(17), 6871-6881.

8. Bhandari, N. R., Day, K. D., Payakachat, N., Franks, A. M., McCain, K. R., & Ragland, D. (2018). Use and Risk Perception of Electronic Nicotine Delivery Systems and Tobacco in Pregnancy. Womens Health Issues, 28(3), 251-257. doi:10.1016/j.whi.2018.02.005

9. Cervellati, F., Muresan, X. M., Sticozzi, C., Gambari, R., Montagner, G., Forman, H. J., . . . Valacchi, G. (2014). Comparative effects between electronic and cigarette smoke in human keratinocytes and epithelial lung cells. Toxicol In Vitro, 28(5), 999-1005. doi:10.1016/j.tiv.2014.04.012

10. Chen, H., Li, G., Chan, Y. L., Chapman, D. G., Sukjamnong, S., Nguyen, T., . . . Oliver, B. G. (2018). Maternal E-Cigarette Exposure in Mice Alters DNA Methylation and Lung Cytokine Expression in Offspring. Am J Respir Cell Mol Biol, 58(3), 366-377. doi:10.1165/rcmb.2017-0206RC

11. Chun, L. F., Moazed, F., Calfee, C. S., Matthay, M. A., & Gotts, J. E. (2017). Pulmonary toxicity of e-cigarettes. Am J Physiol Lung Cell Mol

Physiol, 313(2), L193-L206. doi:10.1152/ajplung.00071.2017

12. England, L. J., Aagaard, K., Bloch, M., Conway, K., Cosgrove, K., Grana, R., . . . Wakschlag, L. (2017). Developmental toxicity of nicotine: A transdisciplinary synthesis and implications for emerging tobacco products. Neurosci Biobehav Rev, 72, 176-189. doi:10.1016/j.neubiorev.2016.11.013

13. Evereklioglu, C., Ozkiriş, A., Alaşehirli, B., Sari, I., Güldür, E., Cengiz, B., & Kontaş, O. (2003). Effect of gestational nicotine treatment on newborn rat retina: a histopathological and morphometric analysis. Ophthalmic Physiol Opt, 23(6), 527-533.

14. Farsalinos, K. E., Romagna, G., Allifranchini, E., Ripamonti, E., Bocchietto, E., Todeschi, S., . . . Voudris, V. (2013). Comparison of the cytotoxic potential of cigarette smoke and electronic cigarette vapour extract on cultured myocardial cells. Int J Environ Res Public Health, 10(10), 5146-5162. doi:10.3390/ijerph10105146

15. Goniewicz, M. L., Knysak, J., Gawron, M., Kosmider, L., Sobczak, A., Kurek, J., . . . Benowitz, N. (2014). Levels of selected carcinogens and toxicants in vapour from electronic cigarettes. Tob Control, 23(2), 133-139. doi:10.1136/tobaccocontrol-2012-050859

16. Hamer, M., Ford, T., Stamatakis, E., Dockray, S., & Batty, G. D. (2011). Objectively measured secondhand smoke exposure and mental health in children: evidence from the Scottish Health Survey. Arch Pediatr Adolesc Med, 165(4), 326-331. doi:10.1001/archpediatrics.2010.243

17. Hudy, M. H., Traves, S. L., Wiehler, S., & Proud, D. (2010). Cigarette smoke modulates rhinovirus-induced airway epithelial cell chemokine production. Eur Respir J, 35(6), 1256-1263. doi:10.1183/09031936.00128809

18. Jang, M. H., Shin, M. C., Jung, S. B., Lee, T. H., Bahn, G. H., Kwon, Y. K., . . . Kim, C. J. (2002). Alcohol and nicotine reduce cell proliferation and enhance apoptosis in dentate gyrus. Neuroreport, 13(12), 1509-1513.

19. Jensen, R. P., Luo, W., Pankow, J. F., Strongin, R. M., & Peyton, D. H. (2015). Hidden formaldehyde in e-cigarette aerosols. N Engl J Med, 372(4), 392-394. doi:10.1056/NEJMc1413069

20. Jordanov, J. S. (1990). Cotinine concentrations in amniotic fluid and urine of smoking, passive smoking and non-smoking pregnant women at term and in the urine of their neonates on 1st day of life. Eur J Pediatr, 149(10), 734-737.

21. Kaur, G., Muthumalage, T., & Rahman, I. (2018). Mechanisms of toxicity and biomarkers of flavoring and flavor enhancing chemicals in emerging tobacco and non-tobacco products. Toxicol Lett, 288, 143-155. doi:10.1016/j.toxlet.2018.02.025

22. Kennedy, A. E., Kandalam, S., Olivares-Navarrete, R., & Dickinson, A. J. G. (2017). E-cigarette aerosol exposure can cause craniofacial defects in Xenopus laevis embryos and

mammalian neural crest cells. PLoS One, 12(9), e0185729. doi:10.1371/journal.pone.0185729

23. Kurti, A. N., Redner, R., Lopez, A. A., Keith, D. R., Villanti, A. C., Stanton, C. A., . . . Higgins, S. T. (2017). Tobacco and nicotine delivery product use in a national sample of pregnant women. Prev Med, 104, 50-56. doi:10.1016/j.ypmed.2017.07.030

24. Köhler, E., Avenarius, S., Rabsilber, A., Gerloff, C., & Jorch, G. (2010). Nicotine and its metabolites in amniotic fluid at birth--assessment of prenatal tobacco smoke exposure. Hum Exp Toxicol, 29(5), 385-391. doi:10.1177/0960327110363326

25. Law, K. L., Stroud, L. R., LaGasse, L. L., Niaura, R., Liu, J., & Lester, B. M. (2003). Smoking during pregnancy and newborn neurobehavior. Pediatrics, 111(6 Pt 1), 1318-1323.

26. Massarsky, A., Abdel, A., Glazer, L., Levin, E. D., & Di Giulio, R. T. (2018). Neurobehavioral effects of 1,2-propanediol in zebrafish (Danio rerio). Neurotoxicology, 65, 111-124. doi:10.1016/j.neuro.2018.02.007

27. Mechawar, N., Saghatelyan, A., Grailhe, R., Scoriels, L., Gheusi, G., Gabellec, M. M., . . . Changeux, J. P. (2004). Nicotinic receptors regulate the survival of newborn neurons in the adult olfactory bulb. Proc Natl Acad Sci U S A, 101(26), 9822-9826. doi:10.1073/pnas.0403361101

28. Menelaou, E., Paul, L. T., Perera, S. N., & Svoboda, K. R. (2015). Motoneuron axon pathfinding errors in zebrafish: differential effects related to concentration and timing of nicotine exposure. Toxicol Appl Pharmacol, 284(1), 65-78. doi:10.1016/j.taap.2015.01.022

29. Nawrocki, L. W. (1985). Development of the neural retina in the zebrafish, Brachydanio rerio.

30. Otręba, M., Kośmider, L., Knysak, J., Warncke, J. D., & Sobczak, A. (2018). E-cigarettes: voltage- and concentration-dependent loss in human lung adenocarcinoma viability. J Appl Toxicol. doi:10.1002/jat.3625

31. Pagani, L. S. (2014). Environmental tobacco smoke exposure and brain development: the case of attention deficit/hyperactivity disorder. Neurosci Biobehav Rev, 44, 195-205. doi:10.1016/j.neubiorev.2013.03.008

32. Palpant, N. J., Hofsteen, P., Pabon, L., Reinecke, H., & Murry, C. E. (2015). Cardiac development in zebrafish and human embryonic stem cells is inhibited by exposure to tobacco cigarettes and e-cigarettes. PLoS One, 10(5), e0126259. doi:10.1371/journal.pone.0126259

33. Pittman, A. J., Law, M. Y., & Chien, C. B. (2008). Pathfinding in a large vertebrate axon tract: isotypic interactions guide retinotectal axons at multiple choice points. Development, 135(17), 2865-2871. doi:10.1242/dev.025049

34. Poorthuis, R. B., Goriounova, N. A., Couey, J. J., & Mansvelder, H. D. (2009). Nicotinic actions on neuronal networks for cognition: general principles and long-term consequences. Biochem Pharmacol, 78(7), 668-676. doi:10.1016/j.bcp.2009.04.031

35. Pugh, P. C., & Berg, D. K. (1994). Neuronal acetylcholine receptors that bind alpha-bungarotoxin mediate neurite retraction in a calcium-dependent manner. J Neurosci, 14(2), 889-896.

36. Putzhammer, R., Doppler, C., Jakschitz, T., Heinz, K., Förste, J., Danzl, K., . . . Bernhard, D. (2016). Vapours of US and EU Market Leader Electronic Cigarette Brands and Liquids Are Cytotoxic for Human Vascular Endothelial Cells. PLoS One, 11(6), e0157337. doi:10.1371/journal.pone.0157337

37. Romagna, G., Allifranchini, E., Bocchietto, E., Todeschi, S., Esposito, M., & Farsalinos, K. E. (2013). Cytotoxicity evaluation of electronic cigarette vapor extract on cultured mammalian fibroblasts (ClearStream-LIFE): comparison with tobacco cigarette smoke extract. Inhal Toxicol, 25(6), 354-361. doi:10.3109/08958378.2013.793439

38. Roy, T. S., Seidler, F. J., & Slotkin, T. A. (2002). Prenatal nicotine exposure evokes alterations of cell structure in hippocampus and somatosensory cortex. J Pharmacol Exp Ther, 300(1), 124-133.

39. Scheffler, S., Dieken, H., Krischenowski, O., & Aufderheide, M. (2015). Cytotoxic Evaluation of e-Liquid Aerosol using Different Lung-Derived Cell Models. Int J Environ Res Public Health, 12(10), 12466-12474. doi:10.3390/ijerph121012466

40. Singh, J., Luquet, E., Smith, D. P. T., Potgieter, H. J., & Ragazzon, P. (2016). Toxicological and analytical assessment of e-cigarette refill components on airway epithelia. Sci Prog, 99(4), 351-398. doi:10.3184/003685016X14773090197706

41. Slotkin, T. A., Skavicus, S., Card, J., Stadler, A., Levin, E. D., & Seidler, F. J. (2015). Developmental Neurotoxicity of Tobacco Smoke Directed Toward Cholinergic and Serotonergic Systems: More Than Just Nicotine. Toxicol Sci, 147(1), 178-189. doi:10.1093/toxsci/kfv123

42. Slotkin, T. A., Stadler, A., Skavicus, S., Card, J., Ruff, J., Levin, E. D., & Seidler, F. J. (2017). Is There a Critical Period for the Developmental Neurotoxicity of Low-Level Tobacco Smoke Exposure? Toxicol Sci, 155(1), 75-84. doi:10.1093/toxsci/kfw180

43. Svoboda, K. R., Vijayaraghavan, S., & Tanguay, R. L. (2002). Nicotinic receptors mediate changes in spinal motoneuron development and axonal pathfinding in embryonic zebrafish exposed to nicotine. J Neurosci, 22(24), 10731-10741.

44. Tegin, G., Mekala, H. M., Sarai, S. K., & Lippmann, S. (2018). E-Cigarette Toxicity? South Med J, 111(1), 35-38. doi:10.14423/SMJ.0000000000000749

45. van der Eijk, Y., Petersen, A. B., & Bialous, S. A. (2017). E-cigarette use in pregnancy: a human rights-based approach to policy and practice. Acta Obstet Gynecol Scand, 96(11), 1283-1288. doi:10.1111/aogs.13198

46. Wagner, N. J., Camerota, M., & Propper, C. (2017). Prevalence and Perceptions of Electronic Cigarette Use during Pregnancy. Matern Child

Health J, 21(8), 1655-1661. doi:10.1007/s10995-016-2257-9

47. Wang, Y., Wang, L., Zhu, Y., & Qin, J. (2018). Human brain organoid-on-a-chip to model prenatal nicotine exposure. Lab Chip, 18(6), 851-860. doi:10.1039/c7lc01084b

48. Welsh, L., Tanguay, R. L., & Svoboda, K. R. (2009). Uncoupling nicotine mediated motoneuron axonal pathfinding errors and muscle degeneration in zebrafish. Toxicol Appl Pharmacol, 237(1), 29-40. doi:10.1016/j.taap.2008.06.025

49. Westerfield, M. (2007). The Zebrafish Book. A Guide for the Laboratory Use of Zebrafish (Danio rerio) (5th ed.). Eugene: University of Oregon.

50. Yolton, K., Khoury, J., Xu, Y., Succop, P., Lanphear, B., Bernert, J. T., & Lester, B. (2009). Low-level prenatal exposure to nicotine and infant neurobehavior. Neurotoxicol Teratol, 31(6), 356-363. doi:10.1016/j.ntt.2009.07.004

51. Zheng, J. Q., Felder, M., Connor, J. A., & Poo, M. M. (1994). Turning of nerve growth cones induced by neurotransmitters. Nature, 368(6467), 140-144. doi:10.1038/368140a0

52. Zhu, J., Fan, F., McCarthy, D. M., Zhang, L., Cannon, E. N., Spencer, T. J., . . . Bhide, P. G. (2017). A prenatal nicotine exposure mouse model of methylphenidate responsive ADHD-associated cognitive phenotypes. Int J Dev Neurosci, 58, 26-34. doi:10.1016/j.ijdevneu.2017.01.014.

Change in Bone Density Following Vitamin D Supplementation in a Pilot Cohort of Older Adults

Haugan, D.N. [1,2], Burt, L.A. [1], Gabel, L. [1], Billington, E.O. [1], Hanley, D.A. [1], Boyd, S.K. [1]

[1]McCaig Institute for Bone and Joint Health, Cumming School of Medicine, University of Calgary, 3280 Hospital Dr. NW, Calgary, AB, Canada, T2N4Z6

[2]Faculty of Engineering, University of Victoria, 3800 Finnerty Rd., Victoria, BC, Canada, V8P5C2

ABSTRACT

Vitamin D supplementation may positively influence bone health, although results are inconclusive. The ideal vitamin D dose for optimal bone health remains controversial. The influence of three years of vitamin D supplementation of varying doses on areal bone mineral density (aBMD) and trabecular bone score (TBS) in older adults is currently unknown. Therefore, the aim of this study was to explore longitudinal changes of aBMD and TBS following three years of vitamin D supplementation in a pilot cohort of older adults. This study reports on the pilot cohort from a large randomized control trial to determine the effect of vitamin D supplementation on bone density. 62 participants completed screening and were randomized to receive dosages of 400 (n =15), 4000 (n = 25), or 10,000 (n = 22) IU daily of vitamin D. aBMD and TBS measures were assessed through dual X-ray absorptiometry (DXA) scans of the hip, lumbar spine, and radius at four time points (baseline, month 12, 24, 36). Repeated measures ANOVA compared group mean aBMD and TBS values over time. Statistics were performed using R. 56 participants completed all study visits (men: 17; women: 39). The average age of the participants was 62.5 ($\pm$4.0) years. Neither aBMD nor TBS showed a significant relationship between vitamin D supplementation group and study duration ($p > 0.05$). No between-group differences were observed. This pilot study suggests that vitamin D supplementation is not related to changes in aBMD and TBS over three years.

KEYWORDS

bone mineral density, dual X-ray absorptiometry, osteoporosis, randomized controlled trial, trabecular bone score, vitamin D

INTRODUCTION

Dual X-ray absorptiometry (DXA) is an accurate, precise, and reproducible 2D tool used to assess bone. DXA scans can provide information about a variety of bone health variables, including areal bone mineral density (aBMD, g/cm^2), bone mineral content, and fracture risk. aBMD, the bone mineral content per unit area found in DXA images is used alongside the World Health Organization's T-score for osteoporosis diagnosis (T-score $\leq$ -2.5) and categorically identifying fracture risk (Unnanuntana, Gladnick, Donnelly, & Lane, 2010). T-score represents the standard deviation by which the aBMD differs from that of a reference population of young adults (Giambini, Dragomir-Daescu, Nassr, Yaszemski, & Zhao, 2016). Trabecular bone score (TBS), a new bone assessment method, is established through a textural variation grey-scale analysis of the pixels in DXA lumbar spine scan images. TBS claims to estimate a 3D structure of the bone segment in an index associated with the trabecular microarchitecture of the vertebrae (Hans, Goertzen, Krieg, & Leslie, 2011). Like aBMD, low TBS values denote clinical risk for fracture. Specifically, non-degraded bone microarchitecture for postmenopausal women with a low risk for fracture would score $\geq$ 1.350 (Silva et al., 2014).

Supplementation of vitamin D of varying dosages has been a controversial subject in many studies, most recommending between 400-1000 IU daily for optimal bone health (Holick et al., 2011), which can be easily attained over-the-counter as a stand-alone supplement or as part of a multivitamin. Without monitoring from a physician, the safe daily upper limit of supplementation has been set at 4000 IU (Holick et al., 2011). Symptoms of toxicity may begin to present with long-term supplementation over 10,000 IU daily (Ross, Taylor, Yaktine, & Del Valle, 2011).

The effects of long term high-dose vitamin D supplementation on aBMD and TBS, in older adults without osteoporosis, are unknown. The aim of this study was to explore longitudinal changes of aBMD and TBS in older adults taking 400, 4000 or 10,000 IU daily of vitamin D for three years. We hypothesized a dose-response relationship in aBMD and TBS with vitamin D supplementation and anticipated that the largest gains would be observed in the 10,000 IU group.

METHODS

Participants

This pilot cohort is part of a large three-year randomized control trial (Burt *et al.*, 2018). Participants in this trial ranged from 55-70 years old and resided close to Calgary, Alberta, Canada. 62 participants, including 44 females and 18 males, qualified for the pilot cohort (the larger randomized control trial enrolled an additional 311 participants). Participants were excluded from this trial if their T-score was $\leq$ -2.5 at the lumbar spine, total hip or femoral neck. Additionally, exclusion occurred if their aBMD classified them as having a high (> 20%) 10-year risk for osteoporotic fracture based on the World Health Organization's Canadian Fracture Risk Assessment tool. Divided at random, three groups were created to receive 400, 4000, or 10,000 IU orally in the form of

vitamin D_3 liquid drops.

Descriptive Variables

We assessed height (m), weight (kg), and blood pressure (mmHg) at each visit using standard methods. We calculated body mass index (BMI) as weight/height^2 (kg/m^2). Body fat percentage was measured with a total body DXA scan. Participants provided information regarding age, sex, ethnicity, and years since last menstrual period in a questionnaire. Serum 25-hydroxyvitamin D [25(OH)D] was measured using a chemiluminescent immunoassay (CLIA) evaluated on a DiaSorin Liaison XL system (DiaSorin, Stillwater, MN).

Bone Assessments

Participants completed DXA scans at baseline, 12, 24, and 36 months. These scans provided values for aBMD, T-score, and TBS. aBMD and T-score were measured at the hip (femoral neck and total hip), lumbar spine and distal radius (ultradistal and 33% radius). TBS was derived using the lumbar spine scan images. All images were assessed by a technologist and reviewed by a trial physician (DH or EB) if abnormalities were identified. Scans with artifacts that precluded accurate interpretation were considered unreportable and excluded from the analysis. Besides having an unreportable lumbar spine, any participant whose BMI was < 15 or > 37 kg/m^2 for all four visits was considered to have unreportable TBS values due to the influence of excessive soft tissue on the TBS analysis software (Medimaps Group, 2012).

Statistical Analysis

Statistical analyses were performed using R (The R Project for Statistical Computing, version 3.5.0). Initial statistics describe baseline demographic characteristics of participants based on randomized group placement. Group mean and standard deviations were found for all variables at each time point. Repeated measures ANOVA showed the significance of the interaction between randomization group, time and the interaction between group and time throughout the study for aBMD, T-score, and TBS. Significance was set at $p < 0.05$. Boxplots show data distribution, medians, and outliers.

RESULTS

A total of 62 participants completed screening and were randomized into three groups to receive 400 (*n*=15), 4000 (*n*=25), 10,000 (*n*=22) IU daily of vitamin D. Baseline descriptives are presented in **Table 1**. Within the original population, 56 (90%) completed all study visits (baseline, month 12, 24, 36).

Table 1. Baseline descriptives of the participants in each randomized group

Variable	400 IU	4,000 IU	10,000 IU
N	15	25	22
Sex (% Female)	80%	72%	64%
Ethnicity (% Caucasian)	93%	84%	82%
Age (yrs)	61.9 (4.2)	62.8 (3.9)	62.7 (4.1)
Height (cm)	170.3 (7.2)	165.2 (6.7)	166.8 (9.9)
Weight (kg)	77.2 (15.5)	70.4 (11.4)	77.6 (18.1)
BMI (kg/m^2)	26.5 (3.7)	25.8 (3.6)	27.7 (5.5)
Years since Menopause (yrs)	11.1 (4.9)	11.0 (5.1)	13.1 (5.5)
Systolic Blood Pressure (mmHg)	126.3 (11.3)	126.3 (15.8)	128.7 (16.5)
Diastolic Blood Pressure (mmHg)	75.9 (5.4)	76.1 (9.3)	77.1 (7.8)
Body Fat (%)	37.1 (6.5)	34.6 (8.2)	36.4 (7.7)
Serum 25(OH)D (nmol/L)	77.2 (16.4)	76.2 (19.4)	75.2 (16.1)

Variables are reported and Mean (SD). 25(OH)D = 25-hydroxyvitamin D

Results from the DXA scans are shown in **Table 2**. Those excluded by study physicians because of unreportable lumbar spines ($n = 7$) were excluded for aBMD, T-score and TBS values. An additional one participant was excluded from the TBS calculation for having a BMI > 37. A total of eight participants were excluded from lumbar spine aBMD, T-score, and TBS analyses. There were no participants with a BMI < 15. Unreportable hips excluded one participant from total hip and femoral neck a BMD and T-score analyses. The repeated measures ANOVA (**Table 2**) showed no significant dependence between vitamin D supplementation group and time for any DXA variable at the 0.05 level. Mean T-scores for all groups show that no group was classified as osteoporotic at any time point (T-score > -2.5). Visual distributions of aBMD and TBS at hip and lumbar spine sites are shown in **Figure. 1**

Table 2. Values for areal bone mineral density, T-score and trabecular bone score at baseline and annual three-year follow-ups and results of group by time interaction from repeated measures analysis of variance (*p value indicates interaction effect (group*time) aBMD: areal Bone Mineral Density; TBS: Trabecular Bone Score)

Variable	Dosage (IU)	Baseline Mean (SD)	12 Months Mean (SD)	24 Months Mean (SD)	36 Months Mean (SD)	p Value*
Total Hip aBMD	400	0.948 (0.118)	0.946 (0.114)	0.940 (0.125)	0.932 (0.125)	1.000
	4,000	0.970 (0.140)	0.966 (0.143)	0.969 (0.145)	0.969 (0.146)	
	10,000	0.995 (0.156)	0.992 (0.168)	0.985 (0.173)	0.980 (0.181)	
Total Hip T-Score	400	-0.487 (0.934)	-0.493 (0.910)	-0.536 (1.000)	-0.593 (0.997)	1.000
	4,000	-0.304 (1.106)	-0.325 (1.132)	-0.309 (1.149)	-0.300 (1.156)	
	10,000	-0.0857 (1.234)	0.121 (1.341)	-0.183 (1.357)	-0.228 (1.445)	
Femoral Neck aBMD	400	0.914 (0.097)	0.907 (0.097)	0.907 (0.109)	0.901 (0.106)	1.000
	4,000	0.890 (0.099)	0.888 (0.107)	0.890 (0.102)	0.893 (0.107)	
	10,000	0.922 (0.133)	0.914 (0.133)	0.910 (0.136)	0.905 (0.140)	
Femoral Neck T-Score	400	-0.887 (0.696)	-0.940 (0.700)	-0.929 (0.790)	-0.979 (0.762)	1.000
	4,000	-1.072 (0.708)	-1.071 (0.765)	-1.065 (0.729)	-1.048 (0.774)	
	10,000	-0.829 (0.957)	-0.879 (0.973)	-0.922 (0.981)	-0.944 (1.017)	
Lumbar Spine aBMD	400	1.204 (0.187)	1.197 (0.175)	1.190 (0.182)	1.190 (0.189)	1.000
	4,000	1.137 (0.171)	1.135 (0.177)	1.142 (0.191)	1.135 (0.200)	
	10,000	1.118 (0.157)	1.144 (0.154)	1.129 (0.163)	1.125 (0.166)	
Lumbar Spine T-Score	400	0.177 (1.530)	0.115 (1.423)	0.0500 (1.493)	0.0500 (1.537)	0.999
	4,000	-0.373 (1.459)	-0.377 (1.495)	-0.300 (1.612)	-0.381 (1.669)	
	10,000	-0.505 (1.284)	-0.300 (1.254)	-0.406 (1.381)	-0.425 (1.387)	
Lumbar Spine TBS	400	1.420 (0.092)	1.382 (0.086)	1.404 (0.087)	1.414 (0.090)	0.978
	4,000	1.394 (0.078)	1.366 (0.084)	1.354 (0.077)	1.378 (0.078)	
	10,000	1.396 (0.098)	1.384 (0.100)	1.372 (0.100)	1.376 (0.106)	
Ultra-distal Radius aBMD	400	0.410 (0.104)	0.409 (0.100)	0.403 (0.107)	0.397 (0.110)	1.000
	4,000	0.425 (0.095)	0.415 (0.098)	0.419 (0.100)	0.412 (0.102)	
	10,000	0.439 (0.106)	0.435 (0.106)	0.436 (0.107)	0.427 (0.101)	
Ultra-distal Radius T-Score	400	-1.467 (1.746)	-1.493 (1.659)	-1.657 (1.826)	-1.800 (1.874)	0.999
	4,000	-1.188 (1.720)	-1.433 (1.809)	-1.370 (1.811)	-1.500 (1.876)	
	10,000	-0.995 (1.890)	-1.150 (1.886)	-1.074 (1.908)	-1.253 (1.793)	
33% Radius aBMD	400	0.832 (0.107)	0.833 (0.109)	0.815 (0.119)	0.827 (0.123)	0.999
	4,000	0.823 (0.125)	0.819 (0.132)	0.820 (0.138)	0.816 (0.141)	
	10,000	0.880 (0.153)	0.890 (0.146)	0.880 (0.147)	0.881 (0.145)	
33% Radius T-Score	400	-0.773 (0.900)	-0.747 (0.937)	-0.971 (1.025)	-0.857 (1.032)	0.999
	4,000	-0.952 (1.109)	-1.013 (1.202)	-1.022 (1.231)	-1.074 (1.276)	
	10,000	-0.455 (1.279)	-0.365 (1.141)	-0.458 (1.176)	-0.442 (1.130)	
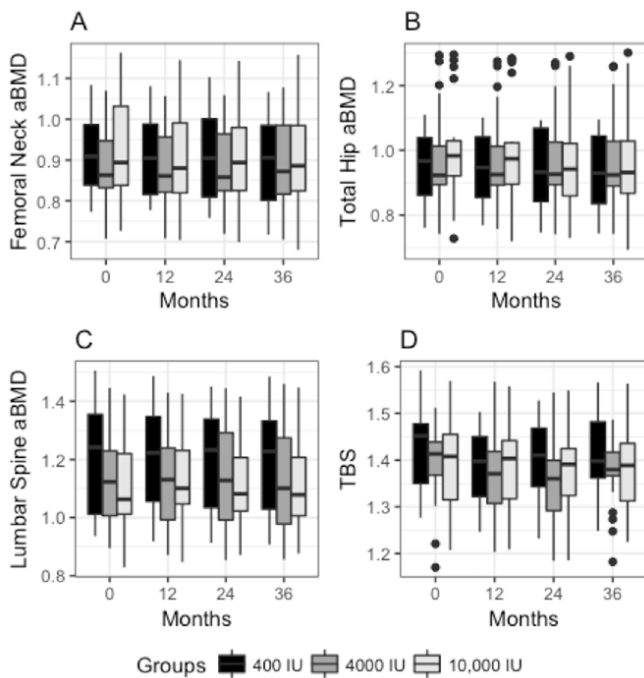
Figure 1. Distributions of: A) femoral neck density B) total hip density C) lumbar spine density D) lumbar spine trabecular bone score at 0, 12, 24, and 36-month time points Boxes show medians and interquartile ranges and the whiskers show the upper and lower interquartile range. aBMD: areal bone mineral density; TBS: trabecular bone score

DISCUSSION

In this study, we investigated the effects of three years of daily supplementation with 400, 4000, and 10,000 IU of vitamin D on aBMD and TBS in older adults. This was the first vitamin D, dose-dependent study to investigate changes longer than one year in aBMD and TBS using DXA. Based on the results, we reject our hypothesis that aBMD and TBS would demonstrate a dose-response relationship following vitamin D supplementation where participants in the 10,000 IU group would see the largest increases.

Due to aBMD being assessed at different skeletal

sites and studies consisting of varying doses of vitamin D, the results of studies evaluating the response of vitamin D supplementation on bone health are often contradictory. Our study showed no significant change in aBMD by supplementation group and time at the total hip, femoral neck, lumbar spine, or distal radius over three years. Our findings are in line with previous longitudinal trials that saw no change in aBMD with supplementation over time at the total hip, lumbar spine (Grimnes *et al.*, 2012; Hansen *et al.*, 2015; Jorde *et al.*, 2010), or femoral neck Cross-sectional studies have also been performed and showed similar results following vitamin D supplementation at the lumbar spine (Fradinger, & Zanchetta, 2001; Marwaha *et al.*, 2011) radius, femoral neck, and hip (Marwaha *et al.*, 2011). However, our findings do not align with multiple cross-sectional studies that saw a positive association between vitamin D serum levels and aBMD of the total hip (Bischoff-Ferrari, Dietrich, Orav, & Dawson-Hughes, 2004), lumbar spine (Collins, Jasani, Fogelman, & Swaminathan, 1998), and femoral neck (Fradinger, & Zanchetta, 2001; Collins *et al.*, 1998).

TBS is a novel technique that estimates trabecular microarchitecture of the lumbar vertebrae (Hans *et al.*, 2011). Due to its novelty, there is currently a lack of comparative studies. Until now, longitudinal studies investigating changes in TBS following vitamin D supplementation in populations of older adults were less than three years and focused on vitamin D insufficient postmenopausal women (Hansen *et al.*, 2015). Few

studies have explored TBS in regards to vitamin D supplementation (Hansen *et al.*, 2015) or serum levels (El Hage, Sebaaly, Issa, Bachour, & Maalouf, 2014), and similar to our results, these studies failed to show any significant influence of supplementation on TBS.

In addition to estimating trabecular microarchitecture, TBS is also thought to be a complimentary means of assessing fracture risk, adding to aBMD's associated T-score through clinical DXA imaging (Schousboe *et al.*, 2016). Like T-score, the numerical index of TBS is suggested to indicate an individual's fracture risk. A score of < 1.350 is indicative of increased fracture risk (Silva *et al.*, 2014). Based on this TBS index, the participants in our study were not at an increased likelihood of osteoporotic fracture and this risk did not change with three years of vitamin D supplementation.

Serum 25-hydroxyvitamin D is used to measure the vitamin D level in the body. Current guidelines classify a serum level of 50-75 nmol/L as representing a sufficient level of vitamin D exposure to prevent vitamin D deficiency and maintain bone health (Holick *et al.*, 2011; Ross *et al.*, 2011). It is possible that our results did not see a positive longitudinal change because our participants entered the study with serum levels in this range. Furthermore, T-score and TBS are considered fracture-risk identifiers with values < -2.5 and < 1.350 (Silva *et al.*, 2014) respectively indicating osteoporotic diagnoses and degraded bone. It is possible that our results for both aBMD and TBS did not see a positive longitudinal change

because mean baseline values for T-score and TBS indicated healthy bone quality. If participants had started the trial with poor bone health (osteoporosis) and or vitamin D deficiency, then there is a possibility that we may have seen more positive results from supplementation throughout the three years.

This study should be considered under the limitation that two lots of the vitamin D drops in the 10,000 IU group experienced degradation. This resulted in dosage variation from 2000-10,000 IU between month 18 and 36 for all participants in this group. This study shows strength in its novelty, three-year length, and randomized-controlled nature. As this was a pilot cohort of a larger study that included a total of 311 participants, it will be interesting to see if the results hold true for the entire main cohort.

CONCLUSION

Three years of vitamin D supplementation had negligible effects on aBMD and TBS regardless of dosage amount. Our results showed no relationship between vitamin D supplementation and DXA measurements of aBMD and TBS over three years. This study is the first to assess the relationship between vitamin D and aBMD and TBS for longer than 1 year. This study will add to the body of literature regarding vitamin D supplementation and its effects on skeletal health. As this was a pilot cohort, it will be interesting to see if these results hold true for the main cohort.

ACKNOWLEDGEMENTS

REFERENCES

1. Bischoff-Ferrari, H. A., Dietrich, T., Orav, E. J., & Dawson-Hughes, B. (2004). Positive Association between 25-Hydroxy Vitamin D Levels and Bone Mineral Density: A Population-Based Study of Younger and Older Adults. *The American Journal of Medicine*, *116*(9), 634–639. https://doi.org/10.1016/j.amjmed.2003.12.029

2. Burt, L. A., Gaudet, S., Kan, M., Rose, M. S., Billington, E. O., Boyd, S. K., & Hanley, D. A. (2018). Methods and procedures for: A randomized double-blind study investigating dose-dependent longitudinal effects of vitamin D supplementation on bone health. *Contemporary Clinical Trials*, *67*, 68–73. https://doi.org/10.1016/j.cct.2018.02.009

3. Collins, D., Jasani, C., Fogelman, I., & Swaminathan, R. (1998). Vitamin D and Bone Mineral Density. *Osteoporosis International : A Journal Established as Result of Cooperation between the European Foundation for Osteoporosis and the National Osteoporosis Foundation of the USA*, *8*(2), 110–114. https://doi.org/10.1007/BF02672505

4. El Hage, R., Sebaaly, A., Issa, M., Bachour, F., & Maalouf, G. (2014). Vitamin D and Trabecular Bone Score in Lebanese Postmenopausal Women. *Journal of Clinical Densitometry*, *17*(3), 404–405. https://doi.org/10.1016/j.jocd.2014.04.026

5. Fradinger, E. E., & Zanchetta., J. R. (2001). Vitamin D and Bone Mineral Density in Ambulatory Women Living in Buenos Aires, Argentina. *Osteoporos. Int.*, *12*(1), 24–27. https://doi.org/10.1007/s001980170153

6. Giambini, H., Dragomir-Daescu, D., Nassr, A., Yaszemski, M. J., & Zhao, C. (2016). Quantitative Computed Tomography Protocols Affect Material Mapping and Quantitative Computed Tomography-Based Finite-Element Analysis Predicted Stiffness. *Journal of Biomechanical Engineering*, *138*(9), 1–7. https://doi.org/10.1115/1.4034172

7. Grimnes, G., Joakimsen, R., Figureenschau, Y., Torjesen, P. A., Almås, B., & Jorde, R. (2012). The effect of high-dose vitamin D on bone mineral density and bone turnover markers in postmenopausal women with low bone mass - A randomized controlled 1-year trial. *Osteoporosis International*, *23*(1), 201–211. https://doi.org/10.1007/s00198-011-1752-5

8. Hans, D., Goertzen, A. L., Krieg, M. A., & Leslie, W. D. (2011). Bone microarchitecture assessed by TBS predicts osteoporotic fractures independent of bone density: The manitoba study. *Journal of Bone and Mineral Research*, *26*(11), 2762–2769. https://doi.org/10.1002/jbmr.499

9. Hansen, K. E., Johnson, R. E., Chambers, K. R., Johnson, M. G., Lemon, C. C., Vo, T. N. T., & Marvdashti, S. (2015). Treatment of Vitamin

D Insufficiency in Postmenopausal Women: A Randomized Clinical Trial. *JAMA Internal Medicine*, *175*(10), 1612–1621. https://doi.org/10.1001/jamainternmed.2015.3874

10. Holick, M. F., Binkley, N. C., Bischoff-Ferrari, H. A., Gordon, C. M., Hanley, D. A., Heaney, R. P., … Weaver, C. M. (2011). Evaluation, Treatment, and Prevention of Vitamin D Deficiency: an Endocrine Society Clinical Practice Guideline. *J. Clin. Endocrinol. Metab.*, *96*(7), 1911–1930. https://doi.org/10.1210/jc.2011-0385

11. Jorde, R., Sneve, M., Torjesen, P. A., Figureenschau, Y., Hansen, J.-B., & Grimnes, G. (2010). No Significant Effect on Bone Mineral Density by High Doses of Vitamin D3 Given to Overweight Subjects for One Year. *Nutrition Journal*, *9*(1), 1. https://doi.org/10.1186/1475-2891-9-1

12. Marwaha, R. K., Tandon, N., Garg, M. K., Kanwar, R., Narang, A., Sastry, A., … Mithal, A. (2011). Bone health in healthy Indian population aged 50 years and above. *Osteoporosis International*, *22*(11), 2829–2836. https://doi.org/10.1007/s00198-010-1507-8

13. Medimaps Group. (2012). TBS insight User Guide.

14. Ross, A. C., Taylor, C. L., Yaktine, A. L., & Del Valle, H. B. (2011). The 2011 report on dietary reference intakes for calcium and vitamin D from the Institute of Medicine: what clinicians need to know. *J. Clin. Endocrinol. Metab.*, *96*(1), 53–58. Retrieved from http://www.nap.edu.

15. Schousboe, J. T., Vo, T., Taylor, B. C., Cawthon, P. M., Schwartz, A. V., Bauer, D. C., … Ensrud, K. E. (2016). Prediction of Incident Major Osteoporotic and Hip Fractures by Trabecular Bone Score (TBS) and Prevalent Radiographic Vertebral Fracture in Older Men. *Journal of Bone and Mineral Research*, *31*(3), 690–697. https://doi.org/10.1002/jbmr.2713

16. Silva, B. C., Leslie, W. D., Resch, H., Lamy, O., Lesnyak, O., Binkley, N., … Bilezikian, J. P. (2014). Trabecular Bone Score: A Noninvasive Analytical Nethod Based Upon the DXA Image. *J. Bone Miner. Res.*, *29*(3), 518–530. https://doi.org/10.1002/jbmr.2176

17. Unnanuntana, A., Gladnick, B. P., Donnelly, E., & Lane, J. M. (2010). The Assessment of Fracture Risk. *The Journal of Bone and Joint Surgery-American Volume*, *92*(3), 743–753. https://doi.org/10.2106/JBJS.I.00919

Consistency of Clinical Risk Factors Associated with Survival in Head and Neck and Lung Cancer Patients

Hongsheng Hu[1], Karen A. Kopciuk[1,2]

[1]Department of Mathematics and Statistics, Faculty of Science, University of Calgary

[2]Department of Cancer Epidemiology and Prevention Research, Alberta Health Services

ABSTRACT

Identifying factors associated with survival following a cancer diagnosis can classify patients at greater or lower risk of death. Cancer stage, race, gender, radiation therapy, smoking status, and age at diagnosis were the risk factors of interest for two types of cancer - head and neck and lung examined in this study. We evaluated whether these risk factors have the same or different association with death from any cause (overall survival) in these cancer types and whether the most commonly used survival model, the Cox Proportional Hazards (PH) model, was the most appropriate choice. Our results found that pathological stage and age at diagnosis increased the risk of death from any cause for both cancer types while radiation therapy decreased this risk, but only for head and neck cancer patients. The Cox PH regression model adequately fit each data set although it was not the most efficient.

KEYWORDS

Cox proportional hazards regression model; Head and Neck Cancer; Kaplan-Meier estimator method; Lung Cancer; Survival analysis; Weibull regression model

INTRODUCTION

Cancer can begin in any cell in the body when there has been a genetic change in a one or a group of cells. These cells will then divide and grow without the usual controls and form a tumour (Trichopoulos, Li, & Hunter, 1996). Squamous cell cancers begin in the tissue that forms the surface of the skin or the lining of the respiratory or digestive tracts resulting in most head and neck (HN) cancers and some lung cancers (LN) (White et al., 2011).

Several factors associated with survival have been identified. In lung squamous cell cancer patients, Savini et al. (2015) found chemotherapy, Eastern Cooperative Oncology Group performance status, gender, and surgery were associated with overall survival (OS). Werner-Wasik and Solan (2006) discovered that disease stage, performance status and weight loss were associated with lung cancer survival. Pilotto et al. (2015) identified age, stage and grade and lymph nodes were important predictors for OS. In head and neck squamous cell cancer patients, Cadoni et al. (2017) found older age and tumour stage were related to OS. Vincent et al. (2012), however, discovered age, comorbidity and tumour size were the most important clinical factors for OS. Thus, there are shared and distinct clinical factors associated with OS in these two types of cancer patients. Although biological and molecular markers are being identified in these patients that can be used for selecting targeted therapies, clinical factors still remain important predictors of survival (Mahar et al., 2015).

The statistical model choice is an important consideration for identifying risk factors associated with survival. In Non-Small Cell Lung Cancer patients, Khaksar, Askarishahi, Hekmatimoghaddam, and Vahedian-Ardakani (2017) found the Cox PH model, which is a semi-parametric model, was not the most efficient statistical model based on the Akaike Information Criterion (AIC); however, this model and the Weibull model identified the same statistically significant risk factors. In gastric cancer patients, Habibi, Rafiei, Chehrei, Shayan, and Tafaqodi (2018) determined that any of the parametric survival models studied including the Weibull model were more efficient than the commonly used Cox PH model and that different statistically significant risk factors were discovered in the various adjusted regression models. Thus, parametric models should be considered, especially if the semi-parametric Cox PH model does not fit the data well (Pourhoseingholi et al., 2011).

OBJECTIVES

The primary objectives of this study are: (1) To assess whether gender, radiation therapy (RT), smoking status, race, age and pathologic stage at diagnosis have the same statistically significant association with overall survival outcomes in both cancer types, and, (2) To determine if the Cox PH model or Weibull regression model are a better fit for each cancer outcome.

METHODS

A comprehensive survival analysis was carried out to evaluate two clinical datasets that recently became available from The Cancer Genome Atlas (TCGA) Research Network (2018). Although

most of the more than 1000 research projects and collaborations have focused on the genomic data for the 33 types of cancer, the clinical and survival data for the two types of squamous cell carcinomas (HN and LN) have not been evaluated to date. Data quality of the two datasets was checked before building survival models by identifying missing data, distributions of continuous variables and sparsity of categorical variable levels. The six clinical risk factors including pathologic stage, gender, RT, smoke, race and age at diagnosis that were common to both data sets were analysed in this study. The Kaplan-Meier estimator method was used to generate survival curves for each single risk indicator with the log-rank test used to assess if there was a statistically significant association with survival.

Multivariable Cox PH and Weibull regression models were then built for each dataset. Since Cox's PH model assumes that the hazard ratio does not depend on time, Schoenfeld residuals plots were made to check this assumption. A Weibull regression model could give an inadequate fit to the dataset if the Weibull distribution assumption is not satisfied. Thus, Cox-Snell (C-S) residuals plots were made to check the goodness fit for each Weibull regression model. For each dataset, a comparison was made between the Cox's PH and the Weibull regression models. Based on model assumptions and goodness of fit checks, a better-fitting survival regression model (either Cox PH or Weibull) was identified for each dataset. Interactions were assessed collectively in each model using a likelihood ratio test and statistical

significance was set at 0.05 for all tests. Analyses were carried out using the R statistical software program (version 3.4.1).

RESULTS

Many aspects of the two cancer datasets are similar. Both have similar sample sizes (N = 492 for LN and N = 526 for HN), proportion of deaths (0.44 for LN and 0.42 for HN), proportion of females (0.26 for LN and 0.27 for HN), are predominately Caucasian (0.71 for LN, 0.86 for HN) and had mostly ex- or current smokers (0.85 for LN and 0.56 for HN; Table 1). However, most LN cancer patients were diagnosed in Stage I (0.49) compared to Stage IV for HN cancer patients (0.51). LN cancer patients seldom received radiation therapy (0.13) whereas HN cancer patients often received it (0.57). The HN patients were about six years younger at diagnosis too (LN mean = 67.3 years vs. HN mean = 60.9 years). The log-rank tests for each risk indicator showed that gender, radiation therapy and age difference had different association with overall survival in the head neck cancer dataset but found no associations in the lung cancer dataset.

For both data sets, significant factors increased the risk (Hazard Ratio > 1) of the outcomes except for RT in the HN data set. Higher pathological stage and older age at diagnosis were associated with increased risk of death in both data sets. Receiving RT significantly reduced the risk of death in the HN data set, where more than half of the patients were given this treatment. Figure 1 shows the results for OS for both data sets.

Both the multivariable Cox PH and the Weibull models gave adequate fits for both cancer datasets and satisfied their respective model assumptions. For the Cox PH model, the PH assumption was not violated and age at diagnoses was linearly related to survival times.

For the Weibull regression model, using the AIC, the Weibull models (1205.8 for LN, 1180.9 for HN) with two more model parameters were still more efficient than the Cox PH models (2281.7 for LN, 2394.9 for HN). The Weibull models fit the observed data well based on the C-S residuals.

Table 1. The frequency (N) and proportion of the patient and tumor categorical characteristics and mean and standard deviation (SD) for Age at Diagnosis in the Lung and Head and Neck (HN) data sets.

	Lung (N=492)			HN (N=526)	
Predictor	N	proportion		N	proportion
Pathologic Stage					
Stage I	240	0.488		27	0.051
Stage II	157	0.32		76	0.14
Stage III	84	0.17		82	0.16
Stage IV	7	0.01		269	0.51
Missing	4	0.008		72	0.14
Gender					
Males	364	0.74		385	0.73
Females	128	0.26		141	0.27
Radiation therapy					
Yes	52	0.13		302	0.57
No	377	0.77		162	0.31
Missing	63	0.13		62	0.12
Race					
Caucasian	350	0.71		451	0.86
Asian	9	0.02		11	0.02
Black or African	30	0.06		48	0.09
American Indian or Alaska Native				2	0.00
Missing	103	0.21		14	0.03
Smoking Status					
Smoker	417	0.85		296	0.56
Nonsmoker	75	0.15		230	0.44
Number of deaths	215	0.44		223	0.42
Number of censored individuals	277	0.56		303	0.58
Age at Diagnosis (Years)					
mean (SD)	67.3	(8.59)		60.96	(11.88
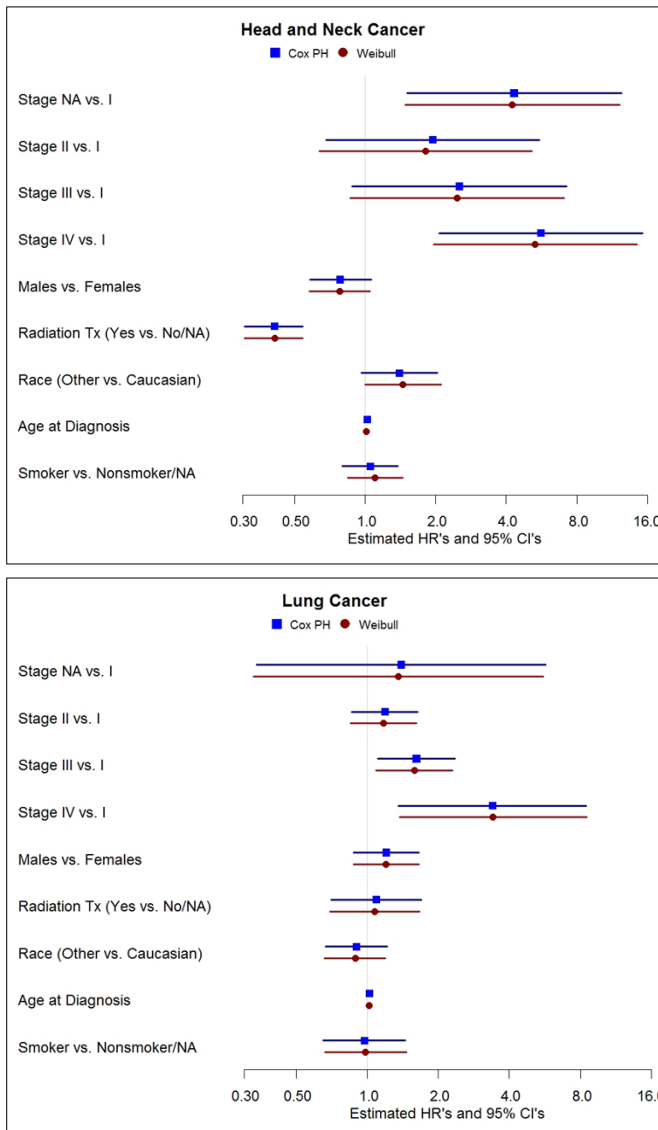
Figure 1. Forest plots showing the estimated Hazard Ratios (HRs) and 95% Confidence Intervals for the Cox PH (blue) and Weibull (red) regression models for OS. The significant factors of higher pathological stages and age at diagnosis have similar HRs that are greater than 1 in both data sets while radiation therapy in the HN data set is substantially less than 1.

DISCUSSION AND CONCLUSION

Pathological stage and age at diagnosis were statistically significant risk factors associated with OS in both HN and LN cancer patients. Pathological stage was also identified by other investigators in HN (Cadoni et al., 2017) and LN

(Werner-Wasik & Solan, 2006; Pilotto et al., 2015) cancer patients as was age at diagnosis in HN (Cadoni et al., 2017; Vincent et al., 2012) and in LN (Pilotto et al., 2015) cancer patients. In LN cancer patients, gender was among the important risk factors in previous research studies (e.g., Pilotto et al., 2015; Savini et al., 2015) but was not in our study. Previous studies included risk factors not available in our data sets, such as performance status, tumour size or patient weight, so these factors could not be evaluated here. Patients receiving RT had a statistically significant decrease in their risk of dying but only if they had a HN cancer. This appears to be a novel finding although as noted above, previous studies did not necessarily include all patient, tumour or treatment factors making full comparisons impossible. The remaining risk factors compared in our study – smoking status, race and gender – were not associated with OS in either data set. In contrast to other studies (e.g., Khaksar et al., 2017; Habibi et al., 2018), both the multivariable Cox PH and Weibull regression models fit the data sets well for both outcomes so either could be used to report findings. However, as noted by previous authors (Khaksar et al., 2017; Habibi et al., 2018; Pourhoseingholi et al., 2011), the Cox PH model was the least efficient by the AIC metric. Use of parametric models, such as the Weibull regression model, in place of the common Cox PH model, is facilitated by programs that can prepare clinically relevant estimated HRs from a fitted parametric model (Zhang, 2016).

In summary, this study identified two well-known

factors were associated with death in two forms of squamous cell cancer (HN, LN) patients and a novel one, RT, for reducing death from HN cancer. Future studies could include common factors to improve comparisons. The traditional method of analysis by a Cox PH regression model was also found to be appropriate for both cancer data sets and met all its model assumptions, although the Weibull regression models were more efficient. Weibull regression models should be considered as a credible alternative to the traditional Cox PH model as often more precise estimates of risk factors are obtained and for ensuring all statistically significant risk factors are identified (Zhu et al., 2011).

ACKNOWLEDGEMENTS

REFERENCES

1. Cadoni, G., Giraldi, L., Petrelli, L., Pandolfini, M., Giuliani, M., Paludetti, G., . . . & Boccia, S. (2017). Prognostic factors in head and neck cancer: A 10-year retrospective analysis in a single-institution in Italy. Acta Otorhinolaryngologica Italica, 37(6), 458.

2. The Cancer Genome Atlas home page (2018). Retrieved from https://cancergenome.nih.gov/

3. Habibi, D., Rafiei, M., Chehrei, A., Shayan, Z., & Tafaqodi, S. (2018). Comparison of survival models for analyzing prognostic factors in gastric cancer patients. Asian Pacific Journal of Cancer Prevention: APJCP, 19(3), 749.

4. Khaksar, E., Askarishahi, M., Hekmatimoghaddam, S., & Vahedian-Ardakani, H. (2017). Cox regression and parametric models: Comparison of how they determine factors influencing survival of patients with non-small cell lung carcinoma. Asian Pacific Journal of Cancer Prevention: APJCP, 18(12), 3389.

5. Mahar, A. L., Compton, C., McShane, L. M., Halabi, S., Asamura, H., Rami-Porta, R., & Groome, P. A. (2015). Refining prognosis in lung cancer: A report on the quality and relevance of clinical prognostic tools. Journal of Thoracic Oncology, 10(11), 1576-1589.

6. Pilotto, S., Sperduti, I., Novello, S., Peretti, U., Milella, M., Facciolo, F., . . ., & Marchetti, A. (2015). Risk stratification model for resected squamous-cell lung cancer patients according to clinical and pathological factors. Journal of Thoracic Oncology, 10(9), 1341-1348.

7. Pourhoseingholi, M. A., Pourhoseingholi, A., Vahedi, M., Dehkordi, B. M., Safaee, A., Ashtari, S., & Zali, M. R. (2011). Alternative for

the Cox regression model: Using parametric models to analyze the survival of cancer patients. Iranian Journal of Cancer Prevention, 4(1).

8. Savini, A., Berardi, R., Mazzanti, P., Caramanti, M., Santoni, M., De Lisa, M., . . . & Onofri, A. (2015). Squamous cell carcinoma of the lung: Clinical criteria for treatment strategy. Journal of Cancer Metastasis and Treatment, Volume, 1(2), 90.

9. Trichopoulos, D., Li, F. P., & Hunter, D. J. (1996). What causes cancer? Scientific American, 275(3), 80-87.

10. Vincent, N., Dassonville, O., Chamorey, E., Poissonnet, G., Pierre, C. S., Nao, E. E. M., ... & Marcy, P. Y. (2012). Clinical and histological prognostic factors in locally advanced oral cavity cancers treated with primary surgery. European annals of otorhinolaryngology, head and neck diseases, 129(6), 291-296.

11. Werner-Wasik, M., & Solan, M. (2006). Clinical prognostic factors in non-small-cell lung cancer. In Syrigos K.N., Nutting C.M., Roussos C. (Eds.), Tumors of the Chest (pp. 177-187). Berlin: Springer.

12. White, A. C., Tran, K., Khuu, J., Dang, C., Cui, Y., Binder, S. W., & Lowry, W. E. (2011). Defining the origins of Ras/p53-mediated squamous cell carcinoma. Proceedings of the National Academy of Sciences, 108(18), 7425-7430.

13. Zhang, Z. (2016). Parametric regression model for survival data: Weibull regression model as an example. Annals of Translational Medicine, 4(24).

14. Zhu, H. P., Xia, X., Chuan, H. Y., Adnan, A., Liu, S. F., & Du, Y. K. (2011). Application of Weibull model for survival of patients with gastric cancer. BMC Gastroenterology, 11(1), 1.

Assessing and Mapping Groundwater Vulnerability to Bacteria in Alberta

Tamara Van Staden*[1], Dr. Edwin Cey[1], Dr. Cathy Ryan[1], Dr. Sylvia Checkley[2,3]

*Department of Environmental Science, University of Calgary, 2500 University Drive NW, Calgary, Alberta, Canada, T2N 1N4

[1]Faculty of Science, University of Calgary, 2500 University Drive NW, Calgary, Alberta, Canada, T2N 1N4

[2]Faculty of Veterinary Medicine, University of Calgary, 1403 29 St NW, Calgary, AB T2N 2T9

[3]Alberta Provincial Laboratory for Public Health, Alberta Health Services, 3030 Hospital Dr NW, T2N 4W4

ABSTRACT

Aquifer vulnerability index methods are commonly used for assessing groundwater vulnerability to surface contaminants. However, the methods have primarily been developed for dissolved contaminants. Microbial contaminants have unique characteristics that result in different transport behavior in the subsurface, and thus require different tools. Key vulnerability factors specific to microbial sources and subsurface transport mechanisms were identified in this study and incorporated into a model using a Geographic Information System framework to create maps of groundwater vulnerability, specific to Escherichia coli, in Alberta for the year 2012. Soil texture, soil organic matter, depth to aquifer, and meteorological conditions were assessed and combined to produce an intrinsic vulnerability map, demonstrating where aquifers were more vulnerable to bacterial contamination. Maps were created for the growing season and cold season, and attempts were made to test the model with E. coli detection data. Statistical analyses revealed the model was not suitable for predictive purposes, which may represent instances where a contamination source was absent, as opposed to real differences in aquifer vulnerability. The results will help decision makers understand which factors should be considered when making a vulnerability map for bacterial contaminants, most notably temporal factors such as precipitation and soil moisture.

KEYWORDS
auifer; contaminant; *E. coli;* GIS; microbial; vulnerability

DEFINITIONS:

Aquifer: a subsurface body of permeable material that holds or transports groundwater.

Vulnerability: a measure of weakness to contamination, or the likelihood of contamination in the event of contaminant exposure.

Contaminant: a substance that can pollute a body of water to the extent that it affects human health.

Microbial: referring to microscopic organism characteristics or behaviour.

E. coli: microorganisms that can indicate the presence of more harmful microorganisms, some strains of *E. coli* are also harmful to humans.

GIS: Geographic Information Systems, a mapping tool used to visually present spatial data.

INTRODUCTION

Groundwater is an important drinking water resource for those who do not have easy access to treated surface water. There are many private residences in Canada, especially in rural areas, that use groundwater as their primary drinking source. Approximately 30% of Canadians and 90% of rural households in Alberta use groundwater as a drinking water resource (Alberta Agriculture and Forestry, 2017; Environment and Climate Change Canada, 2013). The misconception is that groundwater is safe from contamination because of the geology that protects it. However, the infiltration of water contaminated with pathogenic bacteria is possible and these contaminants present a significant risk to human health. An example of this is the Walkerton groundwater contamination tragedy, an incident in which 2,300 residents became ill and seven people died as a result of contamination of well water by microbes (Hrudey,

Payment, Huck, Gillham, & Hrudey, 2003).

Private well users are more exposed to the risks of groundwater contamination, as they usually do not treat their water prior to drinking. The Canadian drinking water guideline for *E. coli* states that none should be detectable per 100 mL of water (Health Canada, 2017), but this is not regulated for private wells, which are most often found in agriculture-dominated regions (Alberta Agriculture and Forestry, 2017). The concern with wells being present in agricultural areas is that health and wellness risks increase with exposure to animal and human sources that potentially contain human pathogens, such as manure fertilizer and septic systems (S A Bradford *et al.*, 2013).

The sensitivity of a groundwater source to contamination by any substance or species is known as aquifer vulnerability (National Research Council, 1993). Vulnerability is based on aquifer characteristics such as the depth to the water table, the material overlying and within the aquifer, and the fate and transport of the contaminant itself. The faster and easier it is for water and contaminants to travel through the subsurface, the greater the intrinsic vulnerability of that aquifer (Dixon & Uddameri, 2016). Vulnerability risk assessment of aquifers has been a prevalent method for determining the health of aquifers and their relative susceptibility to contamination. The assessment can be represented as a map, providing water managers and other stakeholders with a visual indicator of aquifer vulnerability. Most commonly the assessments have been targeted towards dissolved contaminants (e.g. pesticides, nutrients,

heavy metals). The lack of microbial risk assessment can be attributed to the complex characteristics of bacteria, which are living organisms that act as colloidal particles which convolutes otherwise typical fate and transport mechanisms.

This project aims to make an overlay weight of evidence model that has been adapted to include vulnerability factors that specifically relate to bacterial fate and transport, as there are very few models that do this currently. The primary goal of this project was to fill a gap in vulnerability mapping methodology by creating a model to determine the location of shallow aquifers that are intrinsically vulnerable to bacterial contamination.

METHODS

Key vulnerability factors specific to microbial sources and subsurface transport mechanisms were identified and modeled spatially using Geographic Information System (GIS) tools. Intrinsic vulnerability maps for *E. coli* were generated for shallow aquifers in Alberta for the growing season and cold season of 2012. The suitability of the maps was tested by comparing the results with *E. coli* detection data from the same period.

Study Area

The study area was focused on the regions of Alberta where the majority of the population lives (North, South, Central, Foothills, and Peace River regions; **Figure. 1**), and coincides with the agricultural regions of the province where appropriate soil property information is available.
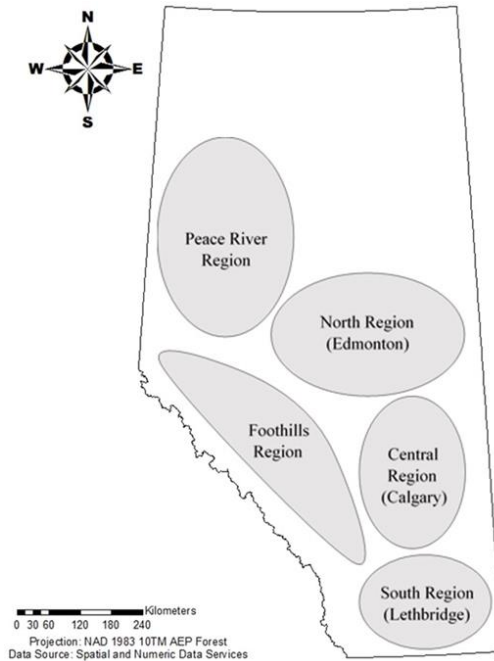
Figure 1. Regions within Alberta where the study was focussed.

Data Description

Six vulnerability factors were selected, including soil moisture, pH, soil texture, soil organic matter, hydraulic resistance, and precipitation. Details and sources regarding the impacts of the factors selected for this model are discussed in Error! Reference source not found.. The cold season and growing season were used to describe seasonal changes and are defined by Alberta Agriculture and Forestry as October 1 - March 31 and April 1 - September 30, respectively. The literature suggests that bacteria survival in the environment is higher in the summer (Charron *et al.*, 2005; Goss, Barry, & Rudolph, 1998; Valeo, Checkley, He, & Neumann, 2016). The most recent precipitation and soil moisture data available prior to a major province-wide flooding event (Pomeroy, Stewart, & Whitfield, 2016) were for the year 2012. The assessment considered only *E. coli* since it is the single most widely used indicator of fecal

contamination (Invik, 2015).

Table 1. List of all the key vulnerability factors, and literature indicating the relationship between the factors and groundwater vulnerability.

Factor	Condition	Effect
Soil Moisture	Low	• Low moisture increases filtration (Corapcioglu & Haridas, 1984)
	High	• More moisture led to more total coliforms (Mellor & Cey, 2015)
Depth to Aquifer	Shallow	• Shallow aquifers are more vulnerable (Cui, Zhou, & Geza, 2016; Pandey, Kass, Soupir, Biswas, & Singh, 2014)
	Deep	• Deeper wells have longer travel times for bacteria and a lower chance of contamination due to die-off (Conboy & Goss, 2000)
Hydraulic Conditions	Generally	• Microbe transport is heavily influenced by aquifer flow (Unc & Goss, 2004) • Flow of groundwater has been is an important consideration for well susceptibility (Conboy & Goss, 2000)
	Low flow	• There is better retention, especially in soils with a small grain size (Scott A. Bradford, Simunek, & Walker, 2006) • No flow can create a sink for biocolloids (Keller & Auset, 2007)
	High flow	• Larger grain size leads to higher hydraulic conductivity, or "velocity enhancement" (Ginn *et al.*, 2002) • Macroporosity increases flow rate which increases pathogen transport (Guber, Shelton, & Pachepsky, 2004) • High velocity decreases straining, leading to a higher output concentration even with small grain size (Scott A. Bradford *et al.*, 2006) • Velocity enhancement decreases with distance (Keller & Auset, 2007)
pH	Low	• Bacteria are negatively charged, so low pH would lead to more adsorption (S A Bradford *et al.*, 2013; Corapcioglu & Haridas, 1984) • There is a lower survival rate of bacteria in lower pH (Sjogren, 1994)
	Neutral	• Quartz has a negative surface charge, metal oxides have a positive surface charge, bacteria are attracted to positive charges (Ginn *et al.*, 2002) • There is less microbe attachment to suspended particles (Guber, Pachepsky, Shelton, & Yu, 2009)
	High	• High pH can mobilize biocolloids in saturated systems (DeNovio, Saiers, & Ryan, 2004) • Biocolloid mobilization is independent of pH (Grolimund & Borkovec, 1999) • There is lower collision efficiency and less attachment in high pH (Schijven, Mülschlegel, Hassanizadeh, Teunis, & de Roda Husman, 2006)
Soil Texture	Generally	• Particle size distribution and clay content influence microbial migration (Butler, Orlob, & Mcgauhey, 1954) • There is no significant difference in transport rates between clay or sand soils in saturated or unsaturated conditions (Safadoust *et al.*, 2011)
	Clay	• Macropores can form in shrinking clay, but otherwise clay has good filtration (Safadoust *et al.*, 2011) • Clay can act as protection for bacteria from UV radiation and antibiotics (Marshall, 1980) • Bacteria survived longer with at least 25% clay in the soil (Burton, Gunnison, & Lanzal, 1987)
	Sand	• Bacteria in sand have optimum retention in saturated conditions (Invik, 2015) • Weathered sand soil has less transport than weathered clay (Invik, 2015) • Sand could have a higher inactivation of *E. coli* than areas without sand (John & Rose, 2005) • Sandy soil has been found to provide protection from *E. coli* contamination (Conboy & Goss, 2000)
Soil Organic Matter		• Bacteria that grow outside of organisms can grow on organic matter, which can be a source of nutrients, thus increasing survival (Corapcioglu & Haridas, 1984) • Organic matter competes with *E. coli* for adsorption space in soil (S A Bradford *et al.*, 2013; Guber *et al.*, 2004; Schijven *et al.*, 2006) • Organic matter also competes with viruses (Sobsey, Dean, Knuckles, & Wagner, 1980) • High concentrations of available carbon can hinder irreversible sorption of bacteria (Marshall, Stout, & Mitchell, 1971)
Precipitation	Low	• Low precipitation would lead to dry conditions, increasing the number of air-water interfaces and increasing the potential for filtration (Corapcioglu & Haridas, 1984)
	Intermittent	• Movement of air-water interfaces increases mobilization (DeNovio *et al.*, 2004)
	High	• More rain increases pathogen numbers in groundwater (Crane & Moore, 1984) • Heavy rainfall will lead to biocolloids reaching the water table faster (S A Bradford *et al.*, 2013; Cey, Rudolph, & Passmore, 2009; Curriero, Patz, Rose, & Lele, 2001)
Seasonal Variations	Generally	• Seasonal changes occur in a triangular wave (Schijven *et al.*, 2006) • August and September have a higher risk of *E. coli* contamination (Invik, 2015)
	Growing Season	• There is more exfiltration (Schijven *et al.*, 2006) • There are more disease outbreaks in summer (Charron *et al.*, 2005; Goss *et al.*, 1998; Valeo *et al.*, 2016)
	Cold Season	• A higher water table and colder water is better for pathogens (Schijven *et al.*, 2006) • A high water table is more vulnerable (Elçi, 2012)

The condition represents the different environmental conditions and properties that define the factor's behaviour (e.g. pH can be

high or low). Note that depth to aquifer and hydraulic conditions influence the hydraulic resistance factor, and seasonal variations are included for informational purposes.

Relative Vulnerability within GIS Layers

Producing a vulnerability map requires the creation of a GIS layer for each factor thought to influence aquifer vulnerability. Each layer was adjusted to reflect the relative impact of that factor on bacteria survival using vulnerability indexes (VIs). Each VI represents the relative influence the factor's variability has on the overall aquifer vulnerability based on literature, data distributions in the current study, and existing regulations. The data in each layer were reclassified and assigned a new value in a GIS layer that had representative areas of high and low vulnerability. Once all the VIs were assigned and the layers were created, the VIs were normalized to give each factor equal weight. The vulnerability layers for each factor were overlain and summed together in GIS to produce an intrinsic bacterial vulnerability map. For an example of the layering system of index methods see *Focazio et al.*, (Focazio, Reilly, Rupert, & Helsel, 1984).

Vulnerability Factors

The details of the VI development for each vulnerability factor are detailed in the following sections and summarized in **Table 2.**

Precipitation

The size of individual precipitation events is important to consider, as large rainfall events are connected to increased disease outbreaks (Curriero *et al.*, 2001). The average event size and the variance of the event sizes at one weather station represent the potential for that location to have large precipitation events. A new precipitation vulnerability indicator, designated P_v, was developed, accounting for the average amount of precipitation per event, P_e, (calculated as total precipitation per season/number of events per season), as well as the variance of the precipitation on days when there was a rain event, V_e. P_v (mm^3/event). was calculated separately for each weather station for both the cold season and the growing season as follows:

$$P_v = P_e \times V_e \qquad \text{(Equation 1)}$$

where P_e represents the average amount of precipitation per event in that season (mm/event), and V_e represents the variance in event size (mm^2).

Precipitation VI values were selected using literature, and patterns observed within the data (**Table 2**). For example, disease outbreaks caused by waterborne pathogens tend to be preceded by large precipitation events that are above the 80th and 90th percentile in size (Curriero *et al.*, 2001).

Soil Moisture

Soil moisture data were obtained as volumetric moisture content (VMC) estimated from plant available water measurements taken across the province. The seasonal average was calculated for each data point. The soil moisture VIs were determined using quartiles, with increasing soil moisture corresponding to an increase in aquifer vulnerability (**Table 2**).

Hydraulic Resistance

The Aquifer Vulnerability Index method uses the thickness of each geological layer above the water

table and the corresponding hydraulic conductivity to calculate hydraulic resistance (Van Stempvoort, Ewert, & Wassenaar, 1993). Hydraulic resistance represents an estimate of protection that overlying geology provides for aquifers (Simpson, Allen, & Journeay, 2014; Van Stempvoort *et al.*, 1993). To account for depth to the water table and hydraulic conductivity, individual well log data from the Alberta Water Well Information Database were used in order to analyze the subsurface geologic properties, as well as the depth to the shallowest aquifer. These data were combined to calculate a hydraulic $R = \sum(d/K)$ resistance value, R (s), for each well with the following formula:

$$(Equation\ 2)$$

where d (m) is the thickness of each geologic layer above the water table, and K (m/s) is the hydraulic conductivity assigned to that geologic material.

Hydraulic conductivities were determined by taking the midpoint of existing hydraulic conductivity ranges for the listed materials (Clapp & Hornberger, 1978; Freeze & Cherry, 1979; Lee, Cho, Kang, & Chun, 2001; Rehm, Groenewold, & Morin, 1980). The VI ranges of hydraulic resistance were determined by using a combination of natural bins in the data, the lower four deciles of the data, and a regulation for wellhead protection zones (**Table 2**) (Moore, 1993).

Soil Texture

Soil texture varies with the proportion of silt, clay, and sand, which is important because it can affect bacterial attachment and movement in the subsurface. For the soil texture vulnerability factor classification, similar classifications used in other vulnerability models were examined (Aller, Lehr, Petty, & Bennett, 1987; Dixon & Uddameri, 2016). The VI values from Dixon & Uddameri, (2016) were used (**Table 2**).

Organic Matter

The presence of organic matter in soil is beneficial to bacteria; increasing OM% increases vulnerability because bacteria are more likely to survive in these conditions (Corapcioglu & Haridas, 1984). The ranges selected by Dixon & Uddameri, (2016) combined with the four quartiles from the data obtained were used to set the VI ranges (**Table 2**).

pH

The pH conditions of the aquifer will affect bacterial mobility and survival, because their ability to grow in population size and survive is highly impacted by pH. VIs were selected using values found in literature (Conner & Kotrola, 1995; Cuthbert, Panes, & Hill, 1955; Madigan *et al.*, 2012; Rudolfs, Falk, & Ragotzkie, 1950; Sjogren, 1994) (**Table 2**).

Table 2. List of ranges and corresponding vulnerability indexes for each factor.

Variable	Range	Vulnerability Index	Additional Comments
Precipitation Variable (mm³/event)	0 – 5.27	1	-
	5.27 – 15.70	2	
	15.70 – 29.53	3	
	29.53 – 186.18	4	
	186.18 – 364.01	5	
	364.01 – 492.64	6	
	492.64+	7	
VMC Range (%)	11.28 – 13.52	1	-
	13.52 – 15.22	2	
	15.22 – 17.67	3	
	17.67 – 22.96	4	
Hydraulic resistance (log₁₀[seconds])			Corresponds to:
	-0.52 – 4.33	4	Minimum – 0.25 days
	4.33 – 5.94	3	0.25 – 10.15 days
	5.94 – 7.54	2	10.15 – 400 days
	7.54+	1	400+ days
Soil Texture	Sandy Loam	8	Values from: Dixon & Uddameri, (2016)
	Loamy Sand	9	
	Sand	10	
	Silt Loam	3	
	Sandy Clay Loam	4	
	Silty Clay Loam	2	
	Loam	5	
	Clay Loam	2	
	Silty Clay	1	
	Clay	1	
	NA	No Data	
Organic Matter (%)	<1.25	1	-
	1.25 – 2.99	2	
	3.00 – 3.99	3	
	4.00 – 54.5	4	
pH Range			Effect:
	0 – 5.5	1	Dangerous for bacteria
	5.5 – 6.9	3	Safe for bacteria
	6.9 – 7.1	4	Optimal for bacteria
	7.1 – 8.3	3	Safe for bacteria
	8.3 – 14.0	2	Moderate for bacteria

Comparison to Microbial Detection Data and Assignment of Factor Weighting

The model was compared to provincial *E. coli* analyses available from Alberta's voluntary domestic water well sampling program to evaluate which factors had a stronger correlation to microbial presence in the subsurface. The *E. coli* detection data used were provided by the Alberta Provincial Laboratory for Public Health (ProvLab), Alberta Health Services. ProvLab receives groundwater samples voluntarily collected by Alberta well owners for bacterial testing and monitoring purposes. All samples were submitted by individuals who requested sampling and followed collection instructions provided. There was no control over where and what time of year

the sample was taken, or the frequency of sampling. The ProvLab dataset for the year 2012 was used and included *E. coli* testing on a total of 8610 samples, of which 155 tested positive for the presence of EC.

Detection and non-detection point data for the year 2012 were used for the comparison. By comparing each layer to *E. coli* detections measured in 2012, a weight could be assigned based on the significance of the correlation. Kruskal-Wallis tests were used to compare the vulnerability values of *E. coli* detection points and non-detect points. If there was a strong correlation between *E. coli* detection and high vulnerability, the factor would be given larger weighting in the final map. Based on the results, further factor adjustment was not warranted. A similar Kruskal-Wallis test was also conducted for the overall vulnerability maps, see Van Staden, (2017).

RESULTS AND DISCUSSION

As described above, an aquifer vulnerability map was created by determining which factors were the most related to *E. coli* detections and combining them in an ArcGIS framework. Six factors were selected based on their data availability and influence on bacteria (**Table 3**). The layers produced for each factor were combined to produce two final vulnerability maps, one for the growing season (**Figure. 2**) and one for the cold season (**Figure. 3**), covering regions where there was available data for all factors.

AQUIFER VULNERABILITY MAPS

The results from the final vulnerability maps gave an indication of where shallow aquifers could be intrinsically vulnerable to bacterial contamination. The overall vulnerability maps had similar patterns for both the growing season (**Figure. 2**) and the cold season (**Figure. 3**). The foothills region of Alberta had the highest vulnerability, while there was lower vulnerability in the central and southern regions. The higher vulnerability in the foothills region is likely driven by the high vulnerability values of both soil moisture and soil organic matter in that region.

The growing season had an overall higher vulnerability than the cold season, which is driven by the higher vulnerability values of precipitation in the growing season (**Figure. 4b**); this is consistent with the observation that more disease outbreaks and higher densities of *E. coli* detections occur in the summer (Charron *et al.*, 2005; Goss *et al.*, 1998; Valeo *et al.*, 2016). Severe weather conditions have been noted as a catalyst for gastrointestinal disease outbreaks, and occur more frequently during summer in temperate regions such as Alberta (Charron *et al.*, 2005; Curriero *et al.*, 2001).

Notable Layers

The precipitation (P_v), soil moisture, and soil organic matter layers were important because they are unique layers that are not used in vulnerability maps for dissolved contaminants. Each of these three layers are naturally linked and gave some insight into what might be causing the patterns visible in the final vulnerability maps. The remaining layers are available in the original work of Van Staden, (2017)**Error! Reference source**

not found..

Precipitation

Patterns for the precipitation layers were very different between the cold season (**Figure. 4a**) and the growing season (**Figure. 4b**). The growing season had the highest vulnerability in the Peace River region. The cold season vulnerability was highest in the mountains and foothills area, although the vulnerability remains relatively low.

The high values in the Peace River region area indicated that there was a higher average precipitation event size, and a larger variance in the event sizes, meaning that there was potential for very large events. Convective weather occurs during a period of the growing season from May to September and results in convective storms that primarily focus on a region extending from Peace River to Rocky Mountain House (Vickers, Buzza, Schmidt, & Mullock, 2001). Summer storms have the potential to occur frequently, and can be large events, which would increase the vulnerability of this area.

The highest cold season P_v occurred in the mountain ranges, which is due to the increased snowfall in the mountains during the winter. However, snow precipitation and soil behaviour in general in the cold season are not likely to increase the vulnerability of shallow aquifers since cold temperatures and the frozen ground decrease infiltration.

Soil Moisture

Soil moisture had similar distributions for both seasons, but there was more overall soil moisture in the growing season (**Figure. 5b**). The regions with the highest soil moisture were the mountains and foothills for both layers. The soil moisture vulnerability in the cold season is overall much lower than in the growing season, which is a result of the ground freezing in the winter (**Figure. 5a**).

The dominant soil type in the high moisture area is Gray Luvisol (Agriculture and Agri-Food Canada, 2005). This soil has a LFH horizon (Litter-Fermented-Humic) that responds quite rapidly to precipitation, increasing soil moisture (Howitt & Pawluk, 1985). The observed pattern of soil moisture could therefore reflect the soil type distribution that exists in Alberta.

Organic Matter

The soil organic matter layer had a large area in the north and foothills regions in the province with a high proportion of organic matter (**Figure. 6**). The central and south regions of the province had less organic matter, and therefore lower vulnerability.

Presence of organic matter within the soil is strongly related to the soil type, and soil type is closely related to ecozones. Both the soil moisture and soil organic matter layers are influenced by climatic and environmental conditions that cause the different ecozones. The conditions within each ecozone influence and are influenced by the amount of soil organic matter, soil moisture, and type of climate in the area. These factors are closely intertwined, and affect each other (Schultz, 2005).

Statistical Comparison to E. coli Detection

Extracted vulnerability values from each factor

layer were compared to *E. coli* detection and non-detection point data using a Kruskal-Wallis statistical test (**Table 4**). The aim was to test the relationship between the vulnerability factor values and the distribution of groundwater *E. coli* detections and non-detections across the province in the year 2012.

The only significant positive correlation for *E. coli* detections were for the cold season soil moisture layer, which suggests that the locations of detections of *E. coli* were accurately predicted by the soil moisture vulnerability values. The other significant result was for the growing season precipitation layer, but more non-detectable *E. coli* values were observed in regions of higher vulnerability, which was the opposite of what was expected.

Sources of Error

The *E. coli* data did not correlate well with the GIS map vulnerability, which could be attributed to several things. Bacterial detection data are not inherently reliable due to the common lack of appropriately frequent sampling rates (Batterman *et al.*, 2009). There are known seasonal patterns in water quality, but most wells lack representative samples throughout the year. The samples tested by ProvLab were primarily obtained from individuals who collected samples from their own private water supply well for monitoring purposes. Some individuals for the year 2012 took regular samples in different months, while others only took samples once that year. Other well owners never sample, potentially introducing a volunteer bias. Another possible reason for the poor correlation could be an absence of a contaminant source at a sampling location, an example of which being if the well was far enough away from a grazing field or stored manure. It is important to remember that the risk of contaminant presence was not considered in this study because the map is intended to represent intrinsic vulnerability.

Model Testing

Aquifer vulnerability map validation can be a complicated and convoluted process, especially if the map covers a large area. Many factors contribute to the location and detection of all types of contaminants, including time lags caused by the travel time of the contaminant, contamination source presence, and the degree of field and lab work required to collect contaminant detection data (Neukum, Hötzl, & Himmelsbach, 2008). A validation was attempted on the unweighted map, but this yielded uncertain and unexpected negative results (**Table 4**). The importance of incorporating risk data (e.g. contaminant sources such as septic tanks) was made apparent through these tests, and could help improve the final map. The map on its own is useful for understanding the spatial distribution of different important factors' influence on bacteria.

Application of the Vulnerability Map

Ultimately, the map produced in this study could not be verified using *E. coli* detection data, and therefore could not be used with certainty for decision making purposes. However, this is the case with several existing vulnerability maps (Eilers & Buckley, 2002). Verification of

vulnerability maps is not often required as they are used as general guides by decision makers as an indication of relative vulnerability. These kinds of maps should not be considered hard evidence of true vulnerability, but rather a suggestion of relative vulnerability of that region in comparison with surrounding regions. The map developed in this study is useful in the sense that it can be used as a guide to estimate relative intrinsic vulnerability of shallow aquifers to bacterial contamination in the Province of Alberta. Individuals and decision makers can use this map to discern whether the site they are on has a vulnerable aquifer; further site-specific aquifer assessments are recommended.

Category	Vulnerability Factor	Effect on Bacteria
Climatic	Precipitation	Mobilization (release from manure and infiltration)
	Soil Moisture	Survival and filtration effects
Geochemical	Organic Matter	Attachment and survival
	pH	Attachment and survival
Geologic	Hydraulic Resistance	Movement through the subsurface, survival, distance to travel in vadose zone
	Soil Texture	Specifically, clay/silt/sand effects on attachment and filtration

Table 3. List of aquifer vulnerability factors and the influence each one would have on bacterial fate and transport.

Table 4. Results of the Kruskal-Wallis tests comparing *E. coli* detection (+) and *E. coli* non-detection (-) point data using spatially corresponding vulnerability values for all factors and the final maps ($p = 0.05$).

Factor	Larger Mean	Larger Median	Significant Less than p (Yes)	Correlation Positive (+)
	(+ or - *E. coli* Detection)		**More than p (No)**	**Negative (-)**
Growing Season Precipitation	-	-	Yes	(-)
Cold Season Soil Moisture	+	Equal	Yes	(+)
Cold Season Precipitation	+	+	No	(+)
Soil Texture	-	Equal	No	(-)
Growing Season Soil Moisture	-	-	No	(-)
Hydraulic Resistance	+	Equal	No	(+)
pH	+	Equal	No	(+)
Organic Matter	-	Equal	No	(-)
Growing Season Overall	-	-	Yes	(-)
Cold Season Overall	+	+	No	(+)
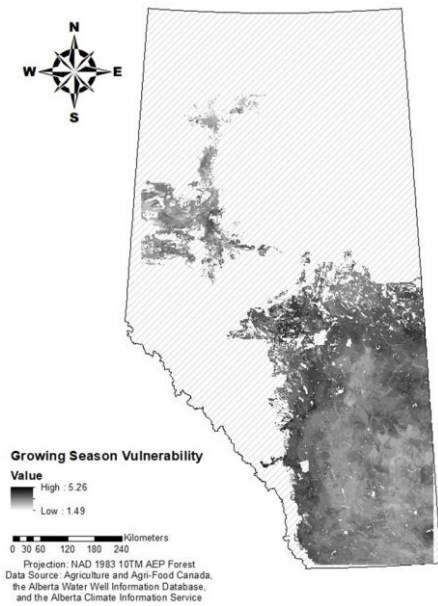
Figure 2. Growing season groundwater bacterial vulnerability map for Alberta, Canada in the year 2012.
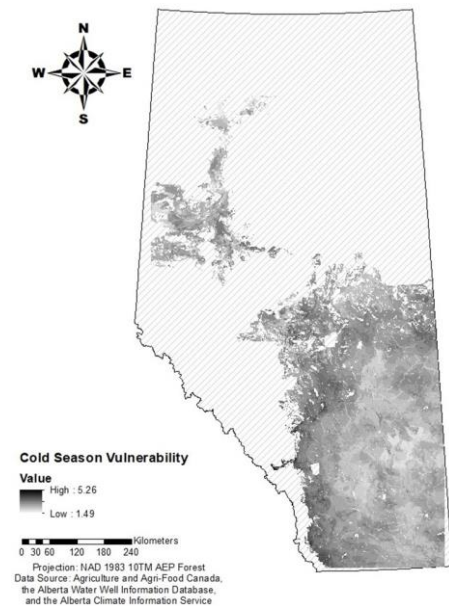

Figure 3. Cold season groundwater bacterial vulnerability map for Alberta, Canada in the year 2012.
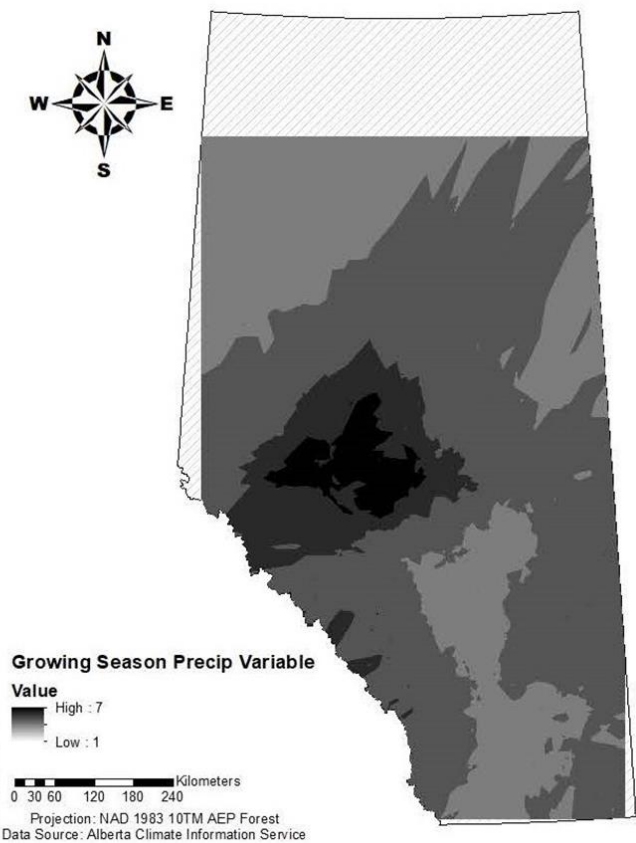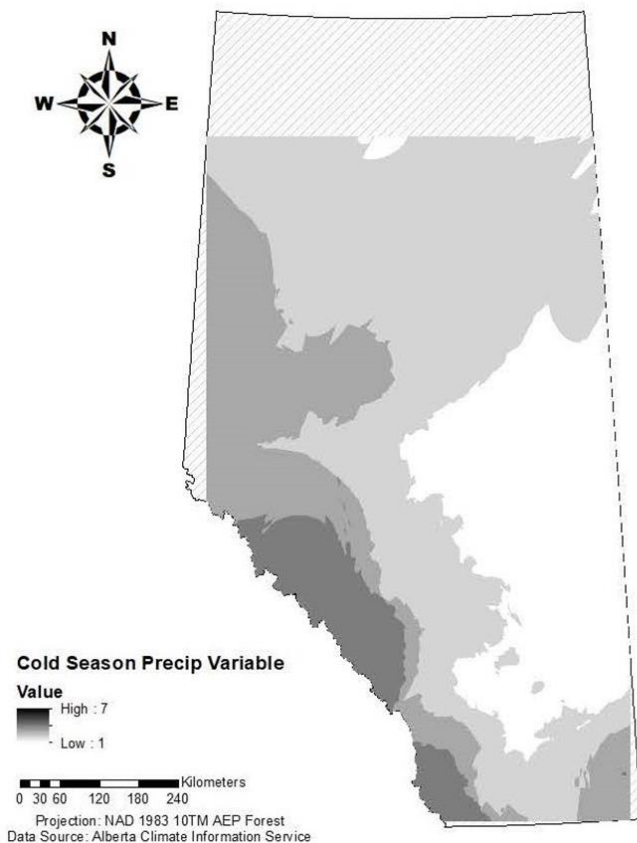
Figure 4. The classified and non-normalized layer for the precipitation variable P_v (mm^2/event) in the cold season (a) and the growing season (b) in Alberta, Canada in the year 2012.
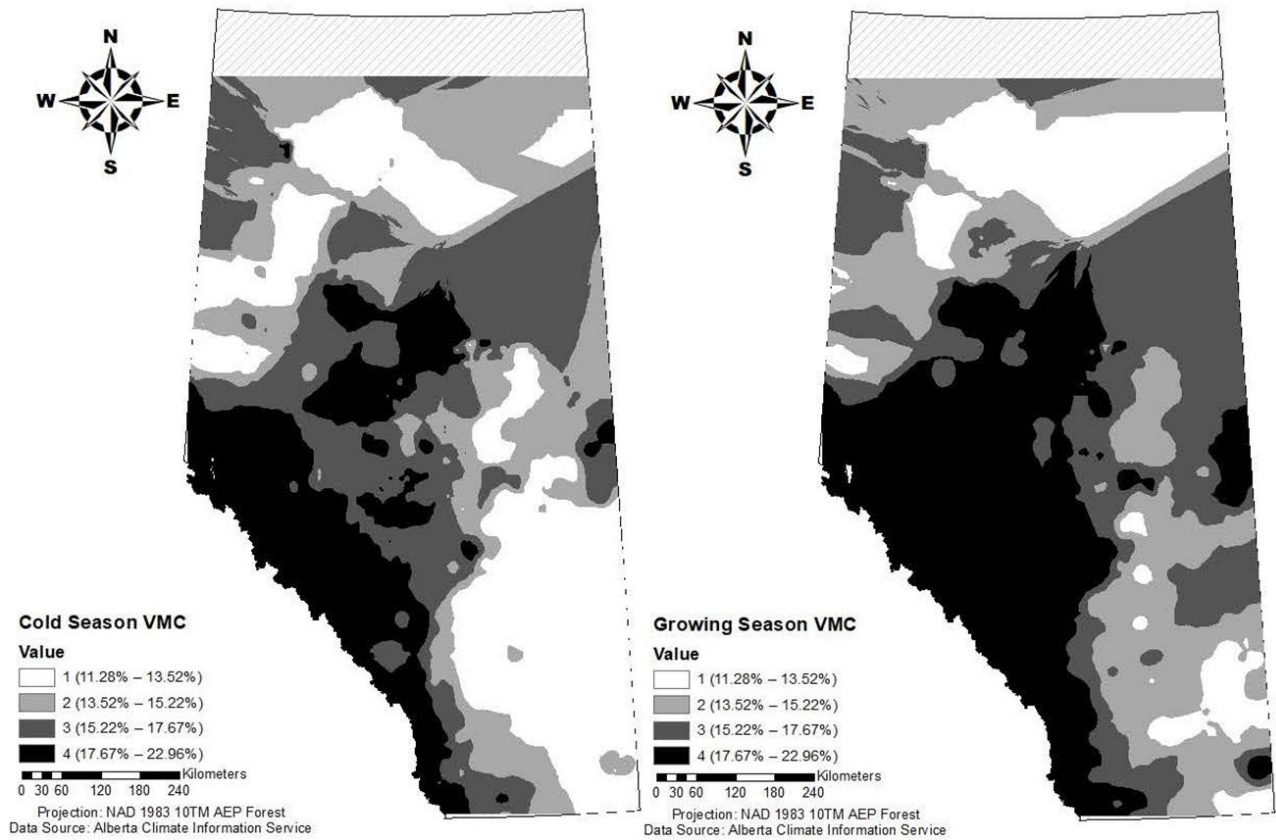
Figure 5. The classified and non-normalized layer for soil moisture as volumetric moisture content (VMC%) in the cold season (a) and the growing season (b) in Alberta, Canada in the year 2012
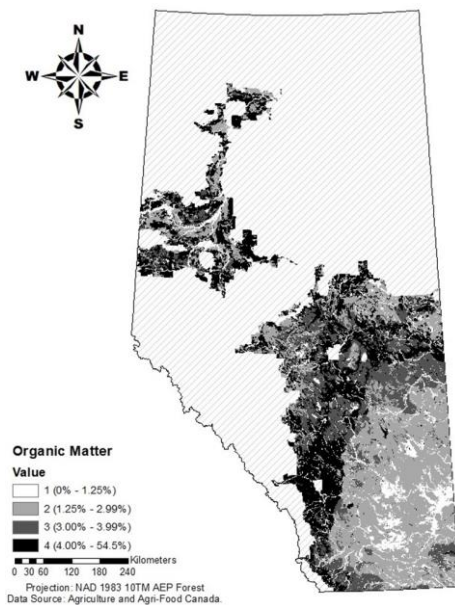
Figure 6. The classified and non-normalized layer for percent soil organic matter in both seasons in Alberta, Canada.

CONCLUSIONS

An intrinsic aquifer vulnerability map for bacterial contaminants was developed by including climatic, soil, and geologic characteristics as vulnerability factors. Climatic factors influence soil conditions, and are not commonly used in vulnerability maps, but are important when considering the fate and transport properties of bacterial contaminants. The inclusion of these factors make this vulnerability map unique.

Although six factors that were thought to be the most relevant for bacterial vulnerability were successfully assembled in this study, only two (cold season soil moisture and growing season precipitation) were found to have a significant relationship to bacterial detection. More tests need to be done that incorporate contaminant sources to further understand the relationship between vulnerability and bacterial detection.

The lack of statistically significant relationships during model testing could be due to the unreliable nature of bacterial data, or the presence/absence of a contaminant source. The statistical analysis of the final map indicated that the model does not have predictive properties, but it could be used to get a basic understanding of intrinsic characteristics and vulnerability.

ACKNOWLEDGEMENTS

REFERENCES

1. Agriculture and Agri-Food Canada. (2005). Soil Groups of Alberta. Retrieved March 10, 2017, from http://www1.agric.gov.ab.ca/$department/deptdocs.nsf/all/agdex10307/$file/pg_14_soil_groups.pdf?OpenElement

2. Alberta Agriculture and Forestry. (2017). Understanding Groundwater. Retrieved May 4, 2017, from http://www1.agric.gov.ab.ca/$department/deptdocs.nsf/all/wwg406

3. Aller, L., Lehr, J. H., Petty, R., & Bennett, T. (1987). DRASTIC: A Standardized System to Evaluate Groundwater Pollution Potential Using Hydrogeologic Settings. National Water Well Association. Worthington, Ohio, United States of America. Retrieved from http://rdn.bc.ca/cms/wpattachments/wpID3175atID5999.pdf

4. Batterman, S., Eisenberg, J., Hardin, R., Kruk, M. E., Lemos, M. C., Michalak, A. M., … Wilson, M. L. (2009). Sustainable control of water-related infectious diseases: A review and proposal for interdisciplinary health-based systems research. Environmental Health Perspectives, 117(7), 1023–1032. https://doi.org/10.1289/ehp.0800423

5. Bradford, S. A., Morales, V. L., Zhang, W., Harvey, R. W., Packman, A. I., Mohanram, A., &

Welty, C. (2013). Transport and fate of microbial pathogens in agricultural settings. Critical Reviews in Environmental Science and Technology, 43(8), 775–893. https://doi.org/10.1080/10643389.2012.710449

6. Bradford, S. A., Simunek, J., & Walker, S. L. (2006). Transport and straining of E. coli O157:H7 in saturated porous media. Water Resources Research, 42(12), 1–12. https://doi.org/10.1029/2005WR004805

7. Burton, G. A., Gunnison, D., & Lanzal, G. R. (1987). Survival of pathogenic bacteria in various freshwater sediments. Applied and Environmental Microbiology, 633–638. Retrieved from http://aem.asm.org/content/53/4/633.full.pdf

8. Butler, R. G., Orlob, G. T., & Mcgauhey, P. H. (1954). Underground movement of bacterial and chemical pollutants. American Water Works Association, 46(2), 97–111. Retrieved from http://www.jstor.org/stable/41253595

9. Cey, E. E., Rudolph, D. L., & Passmore, J. (2009). Influence of macroporosity on preferential solute and colloid transport in unsaturated field soils. Journal of Contaminant Hydrology, 107(1–2), 45–57. https://doi.org/10.1016/j.jconhyd.2009.03.004

10. Charron, D. F., Edge, T., Fleury, M. D., Galatianos, W., Gillis, D., Kent, R., … Waltner-Toews, D. (2005). Links between climate, water and waterborne illness, and projected impacts of climate change. Health Canada. Retrieved from http://inweh.unu.edu/wp-content/uploads/2013/06/252333.pdf

11. Clapp, R. B., & Hornberger, G. M. (1978). Empirical equations for some soil hydraulic properties. Water Resources Research, 14(4), 601–604. https://doi.org/10.1029/WR014i004p00601

12. Conboy, M. J., & Goss, M. J. (2000). Natural protection of groundwater against bacteria of fecal origin. Journal of Contaminant Hydrology, 43(1), 1–24. https://doi.org/10.1016/S0169-7722(99)00100-X

13. Conner, D., & Kotrola, J. (1995). Growth and survival of Escherichia coli O157: H7 under acidic conditions. Applied and Environmental Microbiology, 61(1), 382–385. Retrieved from http://aem.asm.org/content/61/1/382.short

14. Corapcioglu, M. Y., & Haridas, A. (1984). Transport and fate of microorganisms in porous media: A theoretical investigation. Journal of Hydrology, 72(1–2), 149–169. https://doi.org/10.1016/0022-1694(84)90189-6

15. Crane, S. R., & Moore, J. A. (1984). Bacterial pollution of groundwater: A review. Water, Air, and Soil Pollution, 22(1), 67–83.

16. Cui, C., Zhou, W., & Geza, M. (2016). GIS-based nitrogen removal model for assessing Florida's surficial aquifer vulnerability. Environmental Earth Sciences, 75(6), 526. https://doi.org/10.1007/s12665-015-5213-x

17. Curriero, F. C., Patz, J. A., Rose, J. B., & Lele, S. (2001). The association between extreme precipitation and waterborne disease outbreaks in the United States, 1948-1994. American Journal

of Public Health, 91(8), 1194–1199. https://doi.org/10.2105/AJPH.91.8.1194

18. Cuthbert, W. A., Panes, J. J., & Hill, E. C. (1955). Survival of Bacterium coli type I and Streptococcus Faecalis in soil. Journal of Applied Microbiology, 18(3), 408–414.

19. DeNovio, N. M., Saiers, J. E., & Ryan, J. N. (2004). Colloid movement in unsaturated porous media: recent advances and future directions. Vadose Zone Journal, 3(2), 338–351. https://doi.org/10.2113/3.2.338

20. Dixon, B., & Uddameri, V. (2016). Advanced GIS MCDM model coupling for assessing human health risks. In B. Dixon & V. Uddameri (Eds.), GIS and Geocomputation for Water Resource Science and Engineering (pp. 405–426).

21. Eilers, R. G., & Buckley, K. E. (2002). A methodology for evaluating soils, landscapes and geology for nutrient management planning in the Prairie landscape. Retrieved from http://sis.agr.gc.ca/cansis/publications/manuals/2002-hems/hems-2002.pdf

22. Elçi, A. (2012). Advances in GIS-based approaches to groundwater vulnerability assessment: overview and applications. In Clean Soil and Safe Water (pp. 97–114). https://doi.org/10.1007/978-94-007-2240-8

23. Environment and Climate Change Canada. (2013). Groundwater. Retrieved April 4, 2016, from https://www.ec.gc.ca/eau-water/default.asp?lang=En&n=300688DC-1

24. Focazio, M. J., Reilly, T. E., Rupert, M. G., & Helsel, D. R. (1984). Assessing ground-Water vulnerability to contamination: providing scientifically defensible information for decision makers. Retrieved March 31, 2017, from https://pubs.usgs.gov/circ/2002/circ1224/html/new.htm

25. Freeze, A. R., & Cherry, J. A. (1979). Groundwater. Englewood Cliffs, NJ: Prentice-Hall.

26. Ginn, T. R., Wood, B. D., Nelson, K. E., Scheibe, T. D., Murphy, E. M., & Clement, T. P. (2002). Processes in microbial transport in the natural subsurface. Advances in Water Resources, 25(8–12), 1017–1042. https://doi.org/10.1016/S0309-1708(02)00046-5

27. Goss, M. J., Barry, D. A. J., & Rudolph, D. L. (1998). Contamination in Ontario farmstead domestic wells and its association with agriculture: 1. Results from drinking water wells. Journal of Contaminant Hydrology, 32(3–4), 267–293. https://doi.org/10.1016/S0169-7722(98)00054-0

28. Grolimund, D., & Borkovec, M. (1999). Long term release kinetics of colloidal particles from natural porous media. Environmental Science & Technology, 33(22), 4054–4060.

29. Guber, A. K., Pachepsky, Y. A., Shelton, D. R., & Yu, O. (2009). Association of fecal coliforms with soil aggregates: Effect of water content and bovine manure application. Soil Science, 174(10), 543–548. https://doi.org/10.1097/SS.0b013e3181bccc85

30. Guber, A. K., Shelton, D. R., & Pachepsky, Y. A. (2004). Transport and retention of manure-borne

coliforms in soil. Vadose Zone Journal, 4(3), 828–837. https://doi.org/10.2136/vzj2004.0097

31. Health Canada. (2017). Guidelines for Canadian Drinking Water Quality. In Water and Air Quality Bureau, Healthy Environments and Consumer Safety Branch. Ottawa, Ontario.

32. Howitt, R. W., & Pawluk, S. (1985). The genesis of a Gray Luvisol within the Boreal Forest Region. II. dynamic pedology. Canadian Journal of Soil Science, 65, 9–19.

33. Hrudey, S. E., Payment, P., Huck, P. M., Gillham, R. W., & Hrudey, E. J. (2003). A fatal waterborne disease epidemic in Walkerton, Ontario: Comparison with other waterborne outbreaks in the developed world. Water Science and Technology, 47(3), 7–14.

34. Invik, J. (2015). Total coliform and escherichia coli positivity in rural well water in Alberta, Canada: spatiotemporal analysis and risk factor assessment.

35. John, D. E., & Rose, J. B. (2005). Critical review of factors affecting microbial survival in groundwater. Environmental Science & Technology, 39(19), 7345–7356.

36. Keller, A. A., & Auset, M. (2007). A review of visualization techniques of biocolloid transport processes at the pore scale under saturated and unsaturated conditions. Advances in Water Resources, 30(6–7), 1392–1407. https://doi.org/10.1016/j.advwatres.2006.05.013

37. Lee, J. O., Cho, W. J., Kang, C. H., & Chun, K. S. (2001). Swelling and hydraulic properties of Ca-Bentonite for the buffer of a waste repository.

Technologies for the Management of Radioactive Waste from Nuclear Power Plants and Back End Nuclear Fuel Cycle Activities, 1–10. Retrieved from http://www-pub.iaea.org/MTCD/Publications/PDF/csp_006c/PDF-Files/paper-68.pdf

38. Madigan, M. T., Clark, D. P., Martinko, J. M., Stahl, D. A., Bender, K., & Buckley, D. H. (2012). Brock Biology of Microorganisms 13th Edition.

39. Marshall, K. C. (1980). Adsorption of microorganisms to soils and sediments. In G. Bitton & K. C. Marshall (Eds.), Adsorption of Microorganisms to Surfaces (pp. 317–329). Toronto: Wiley.

40. Marshall, K. C., Stout, R., & Mitchell, R. (1971). Mechanism of the initial events in the sorption of marine bacteria to surfaces. Microbiology, 68(3), 337–348. https://doi.org/10.1099/00221287-68-3-337

41. Mellor, A. F. P., & Cey, E. E. (2015). Using generalized additive mixed models to assess spatial, temporal, and hydrologic controls on bacteria and nitrate in a vulnerable agricultural aquifer. Journal of Contaminant Hydrology, 182, 104–116. https://doi.org/10.1016/j.jconhyd.2015.08.010

42. Moore, B. A. (1993). Case studies in wellhead protection area delineation and monitoring.

43. National Research Council. (1993). Ground water vulnerability assessment: predicting relative contamination potential under conditions of uncertainty.

44. Neukum, C., Hötzl, H., & Himmelsbach, T. (2008). Validation of vulnerability mapping methods by field investigations and numerical modelling. Hydrogeology Journal, 16, 641–658. https://doi.org/10.1007/s10040-007-0249-y

45. Pandey, P. K., Kass, P. H., Soupir, M. L., Biswas, S., & Singh, V. P. (2014). Contamination of water resources by pathogenic bacteria. AMB Express, 4(1), 16. https://doi.org/10.1186/s13568-014-0051-x

46. Pomeroy, J. W., Stewart, R. E., & Whitfield, P. H. (2016). The 2013 flood event in the South Saskatchewan and Elk River basins: Causes, assessment and damages. Canadian Water Resources Journal / Revue Canadienne Des Ressources Hydriques, 41(1–2), 105–117. https://doi.org/10.1080/07011784.2015.1089190

47. Rehm, B. W., Groenewold, G. H., & Morin, K. A. (1980). Hydraulic properties of coal and related materials, Northern Great Plains. Ground Water.

48. Rudolfs, W., Falk, L. L., & Ragotzkie, R. A. (1950). Literature review on the occurrence and survival of enteric, pathogenic, and relative prganisms in soil, water, sewage, and sludges, and on vegetation: I. bacterial and virus diseases. Water Environment Federation, 22(10), 1261–1281. https://doi.org/10.1016/S0262-1762(99)80122-9

49. Safadoust, A., Mahboubi, A. A., Gharabaghi, B., Mosaddeghi, M. R., Voroney, P., Unc, A., & Sayyad, G. (2011). Bacterial filtration rates in repacked and weathered soil columns. Geoderma, 167–168, 204–213. https://doi.org/10.1016/j.geoderma.2011.08.014

50. Schijven, J. F., Mülschlegel, J. H. C., Hassanizadeh, S. M., Teunis, P. E. M., & de Roda Husman, A. M. (2006). Determination of protection zones for Dutch groundwater wells against virus contamination - Uncertainty and sensitivity analysis. Journal of Water and Health, 4(3), 297–312. https://doi.org/10.2166/wh.2006.012

51. Schultz, J. (2005). The Ecozones of the World. Springer Berlin Heidelberg.

52. Simpson, M. W. M., Allen, D. M., & Journeay, M. M. (2014). Assessing risk to groundwater quality using an integrated risk framework. Environmental Earth Sciences, 71(11), 4939–4956. https://doi.org/10.1007/s12665-013-2886-x

53. Sjogren, R. E. (1994). Prolonged survival of an environmental Escherchia Coli in laboratory soil microcosms. Water, Air, and Soil Pollution, 75(3), 389–403.

54. Sobsey, M. D., Dean, C. H., Knuckles, M. E., & Wagner, R. A. (1980). Interactions and survival of enteric viruses in soil materials. Applied and Environmental Microbiology, 40(1), 92–101.

55. Unc, A., & Goss, M. J. (2004). Transport of bacteria from manure and protection of water resources. Applied Soil Ecology, 25(1), 1–18. https://doi.org/10.1016/j.apsoil.2003.08.007

56. Valeo, C., Checkley, S., He, J., & Neumann, N. (2016). Rainfall and microbial contamination in Alberta well water. Journal of Environmental Engineering and Science, 11(1), 18–28.

57. Van Staden, T. (2017). Assessing and mapping groundwater vulnerability to bacteria in Alberta. Undergraduate Thesis, University of Calgary. Retrieved from https://dspace.ucalgary.ca:8443/handle/1880/51977

58. Van Stempvoort, D., Ewert, L., & Wassenaar, L. (1993). Aquifer Vulnerability Index: a GIS - compatible method for groundwater vulnerability mapping. Canadian Water Resources Journal, 18(1), 25–37. https://doi.org/10.4296/cwrj1801025

59. Vickers, G., Buzza, S., Schmidt, D., & Mullock, J. (2001). Chapter 3: Weather Patterns of the Prairies. In The Weather of the Canadian Prairies Graphic Area Forecast 32 (pp. 47–67). Ottawa: NAV CANADA and Meteorological Service of Canada. Retrieved from http://www.navcanada.ca/EN/media/Publications /Local Area Weather Manuals/LAWM-Prairies-3-EN.pdf

Design of Electro-Mechanical Underwater Vehicle Engine: An Efficient No-fuel Consuming Substitute for Marine Diesel and Nuclear Engine

Samarpan Deb Majumder

Institute of Engineering & Management, Kolkata, India

ABSTRACT

An efficient passive no-fuel consuming underwater propelling vehicle engine operating only on electricity has been studied in this research. The engine is housing a propeller fan, a compressive body housing a 75KWh rechargeable battery pack, 4 pole 3 phase Induction motor, inverter, an alternator and a single speed transmission 9.73:1 gearbox. The propeller is connected to the motor at the inlet and the turbine at the outlet is connected to the alternator which charges the battery pack. The power is generated by the motor which is transmitted to the shaft connecting the propeller at the inlet, producing around 5990 RPM. The battery is sized according to the rpm delivered by the motor. The theory and concept are derived from the working principle of a scramjet engine, air breathing engine and an Electric Vehicle. All the electrical components are installed inside the compressive body. Efficient charging will occur as the discharge of battery will be regained with the continuous voltage generation by the turbine at the exit. The velocity achieved by the vehicle excluding all losses and drag at its peak working condition is calculated around 32.12m/sec, almost 2 times to that of the speed of conventional underwater running vehicles. The paper analyses the design of Engine, design Calculations, output parameters of Engine, Drop Test, Stress and flow analysis of Engine.

KEYWORDS

Engine; Inverter; Motor; Passive; Scramjet; Underwater

INTRODUCTION

An electric vehicle engine basically comprises of a motor, a generator, a battery, a transmission gear box and other auxiliary components necessary for driving the driver shaft at a higher rpm. The driver shaft drives the driven shaft connecting the wheels for transmission of power. The gear transmission box comprises of a certain gear ratio for reducing the rpm to control the speed. With the rise of regenerative braking, the battery is charged up to a minimal percentage for later use. On the other hand, a diesel engine works under the principle of power derived from combustion and exhaust strokes.

Until now a number of research studies have been performed in the field of underwater vehicles and their control mechanism. Chau et al. (2008), Mcdonal et al. (2008), Xina et al. (2016), Daowd et al. (2012), Berckmans et al. 2012, Fossen et al. (1999), Jimenez et al. (2004) and Mahesh et al. (1991) studied the electrical layout system and the electronic configureuration for vehicle motion underwater. In other studies performed by Bontempo et al. (2018), Shi et al. (2018), Fossen et al. (1991), Healey et al. (1991) and Herman et al. (2009) discussed mechanical studies on how ducting a propeller can improve the performance of a vehicle propelling underwater at different depths and with different velocities. Apart from this study, research works performed by Field et al. (2002), Cristi et al. (1990), Rodrigues (1996), Soylu et al. (2008), Caccia et al. (2000) and Li et al. (2005) developed a study on how the motion of the vehicle at different depth can be controlled in different

conditions. The present research proposal develops a hybrid concept of developing a vehicle which can propel underwater without using any fuel & running only on electricity.

The purpose of this research is to develop an engine employing no combustion engine addressing towards less environmental impact underwater both functionally and economically. An electrical engine tuned with mechanical components is used to obtain higher output parameters in comparison to diesel engines. The heating of the vehicle is also reduced due to the decrease in load on the engine. The mechanical components used are Turbine and a propeller for creating a negative pressure allowing fluid to flow inside the engine, compressive body inspired from that of a scramjet engine to introduce passive compression for high velocity as output. Instead of using a generator, to make the engine less compact and smaller in size, an alternator is used. The alternator rightly fits in the compressive body which will be continuously run by the turbine at the exit. The turbine will therefore rotate the alternator shaft at the required rpm for the desired charge generation in the battery. A 2 pole alternator is used so as to increase the overall rpm and recharge the battery constantly during its running.

In accordance with the proposal, electricity without any dependency on gasoline is used as the driving source for propelling the vehicle. Electricity here is produced by a Battery which drives the 4 pole 3 phase induction motor to propel the vehicle under water. At the standstill condition, electricity from

the lithium ion battery is first converted from DC to AC with the help of an inverter. The AC supply is fed into the motor which employs its rotor to drive the propeller fan at the front of the vehicle at an average speed of 5990 RPM. A Single Speed transmission or a gear box is installed in between the motor and inverter so as to use the power of the motor to drive the propeller. A propeller or a reaction turbine at the outlet is connected to the alternator to charge the battery during its running. The vehicle propelling underwater would not require any friction braking to slow down the vehicle. Hence, cutting off the supply or releasing the acceleration pedal would suffice. The engine is ducted with a certain degree of angle inwards so as to reduce the formation of vortex leading to turbulence at the inlet. The ducting not only improves the performance of the fan blades but also aids in producing additional thrust. The primary design has been inspired from a scramjet engine, but with a turbine at the outlet to further increase the kinetic energy of the liquid passing through. The solid body between the propeller blade and turbine houses the electrical power hub. The diverging converging body in between the propeller and turbine acts as an efficient and a passive compressive device similar to the one used in a scramjet or ramjet engine. The inlet has been installed as diverging so as to optimise supersonic compression and an increase in velocity across the engine. Furthermore, a diverging inlet will maintain a considerably lower inlet to outlet temperature ratio. The electric housing shall be cooled conventionally with direct pass of water over the engine body.

The turbine at the exit upon acceleration will enable the alternator to convert torque to recharge the battery. The average time taken to recharge a battery completely shall be around 1 hour. The duty time for a lithium ion battery on full continuous running condition shall be around 32 hours. The engine housing shall be installed below the vehicle so as to ensure that the centre of gravity always acts below the buoyancy force (lower the centre of gravity, better is the stability of the body underwater). The casing of the hub is converging, thus compelling the engine to act like a nozzle too. The engine will be installed below the vehicle thus pushing the centre of gravity even lower so as to maintain stability underwater. The design of propeller and turbine blades has been achieved on the basis of standard values of angle of attack so as to cater to the drag loss. The taper angle of the compressive body has been accounted on the basis of the increase in velocity of the fluid passing through.

Electrical Engine Layouts

The **Figure 1** illustrates the engine components that will be employed for running the propeller at a specific RPM by creating a suction pressure. Suction pressure here, refers to the negative pressure created for the inflow of water into the engine housing. The battery will serve DC current to the inverter. The inverter will convert DC to AC making it suitable to run the 4 pole 3 phase induction motor. The motor is connected to the shaft via a transmission gear box with a certain gear ratio of 9.73:1 thus reducing the rpm transmitted to the shaft for driving the propeller. **Figure 2** of

Table 1 represents the separate shaft which connects the 2-pole alternator to the turbine at the outlet. The turbine will drive the alternator shaft at a specific speed which will enable the charging of the battery. However, as the rpm at the top working condition is much greater than the rpm of the alternator at the same working condition, "Law of Conservation of Energy" is also satisfied.
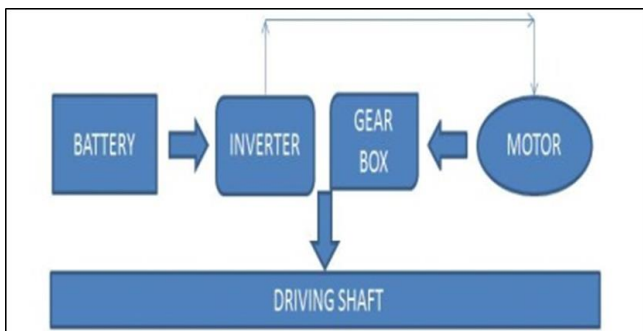
Figure 1. Components connected to the Propeller at the Inlet
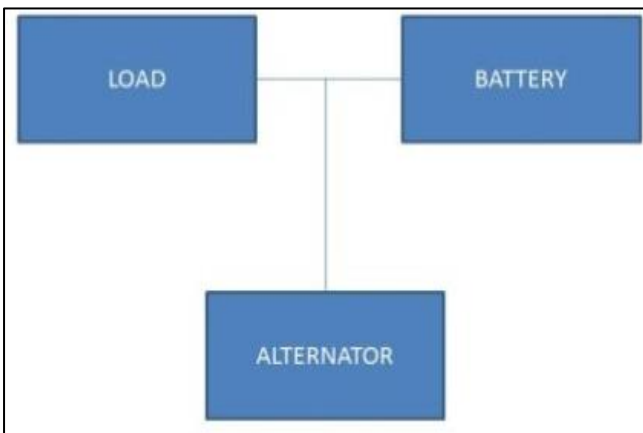
Figure 2. Components connected to the Turbine at the Outlet

Compressive Body

The compressive body at the mid-section of the engine is installed for serving two major purposes:

- Produce ram effect (similar to scramjet engine) to increase the velocity of flow at the outlet of engine.

- House the electrical components like Battery, Inverter, Induction Motor and Single Speed Gear Transmission Box.

This component shall be bolted to the outer casing of the engine, i.e., a duct. For high structural rigidity, high tensile strength, and high compressive strength and to undermine cavitation and corrosion, Alloy C-276 shall be used for its construction. The use of this material will also lengthen the lifetime of the component thus entailing lower running and maintenance cost. The design of the compressive body is depicted in **Figure 3**, **Figure 4** and **Figure 5**.
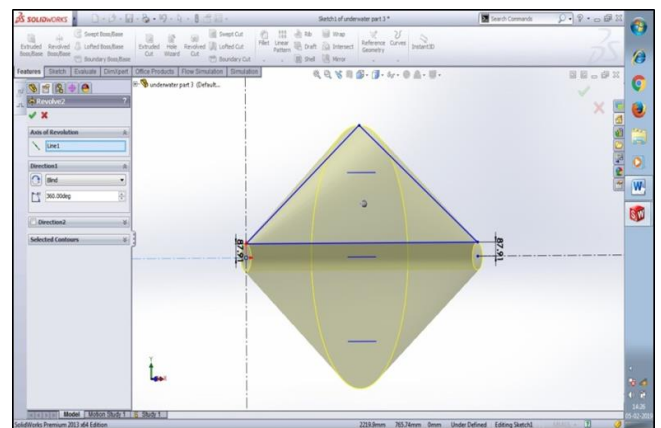
**Figure 3.** Sketch of Compressive Body before Revolved Base
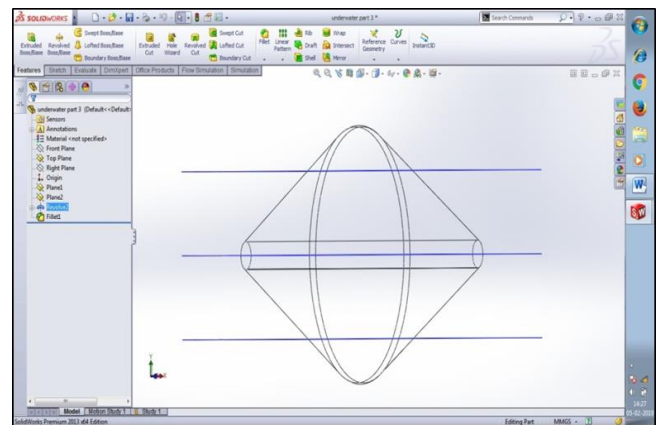

Figure 4. Projection of Compressive Body
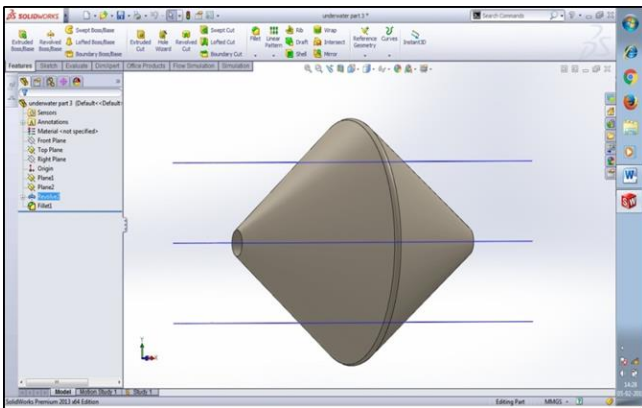
Figure 5. Complete View of Compressive Body

Propeller

The propeller is designed on the basis of Blade Element Momentum Theory. The function of propeller is to create a suction pressure at the inlet for the inflow of water into the engine. The propeller modelling is depicted in **Figure 6** as aerofoil design, **Figure 7** as blade projection up to the required length and **Figure 8** of as the tapering and twisting of blade for required inflow of water.
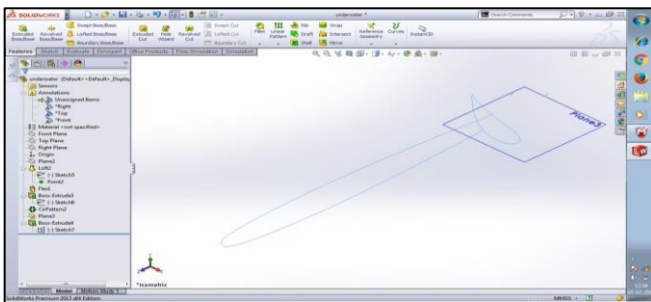
Figure 6. Aerofoil Profile by Blade Element Momentum Theory
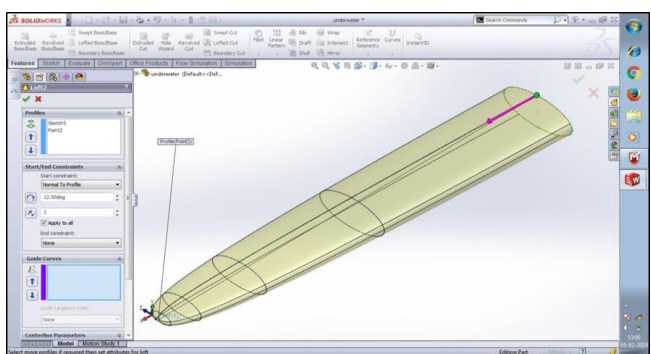
Figure 7. Profile Projection of Propeller Blade
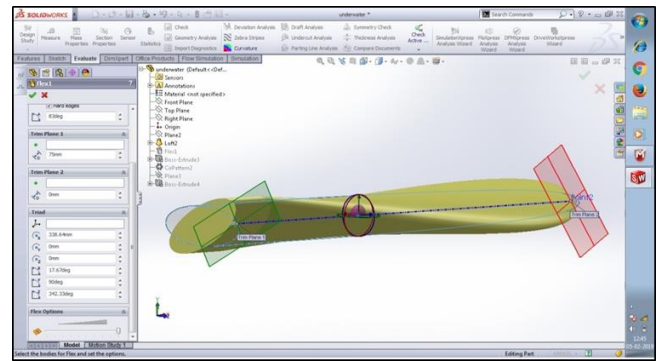
Figure 8. Twist Angle or Projection of Blade after loft
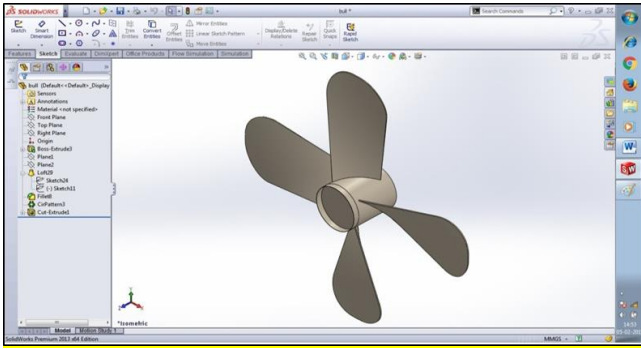
Turbine Blade

The turbine blade is employed to drive the alternator at the outlet for recharging the battery by rotating at a specific speed. **Figure 9**, **Figure 10** and **Figure 11** depict the design of turbine blade for required rpm to the alternator.
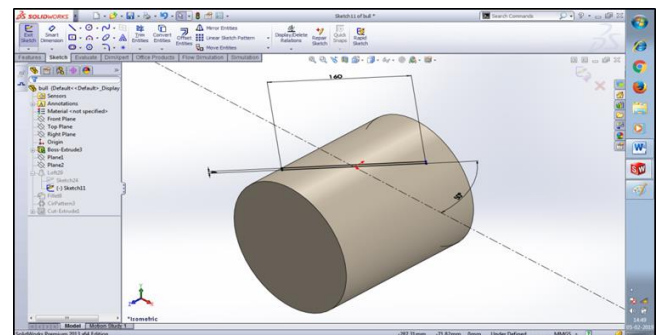
**Figure 9.** Sketch of Turbine Blade
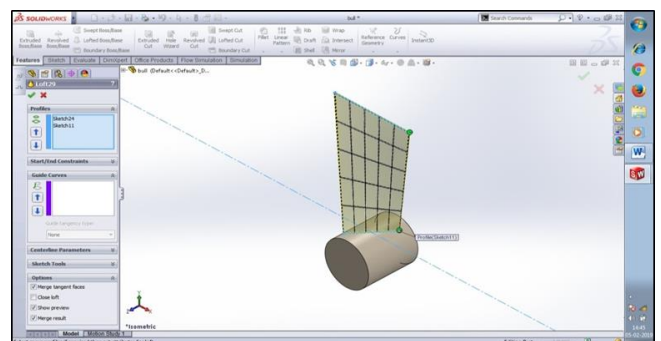

Figure 10. Projection of Turbine Blade

Figure 11. Complete View of Turbine Blade

Engine Housing

The engine housing is having a certain taper angle to ensure no turbulence inside the engine as well as an overall increase in velocity due to the nozzle-like structure. **Figure 12** to **Figure 13** in depicts the hollow design of engine housing with required tapering to avoid turbulence inside the engine and also to increase the overall velocity at the outlet.
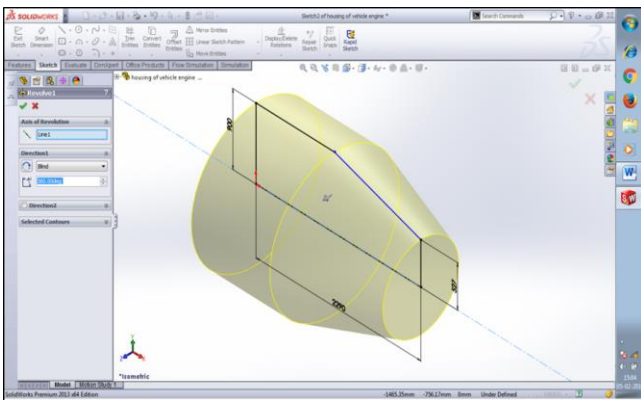

Figure 12. Sketch and Projection of Compressive Body by Revolved Base
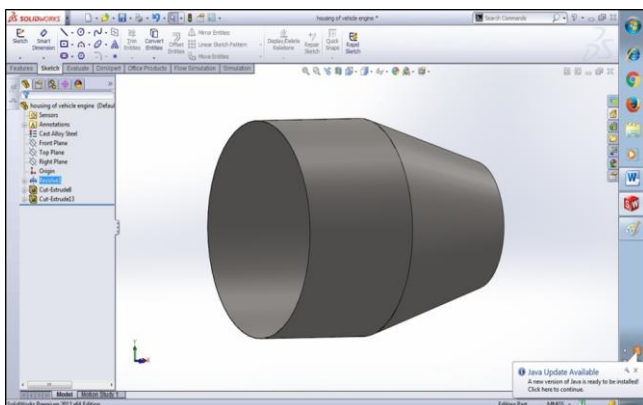

Figure 13. Complete View of Engine Housing

Rear and Front view of the Electric Underwater Propelling Engine

The design is completed in SolidWorks accounting all the standard values for dimensions of Propeller, Turbine Blades, Compressive Body and Shaft as well as the clearance areas of all the sections. The units of dimensions are considered to be in millimeters and the scale has been set to 1:1. The views are illustrated in **Figure 14**.
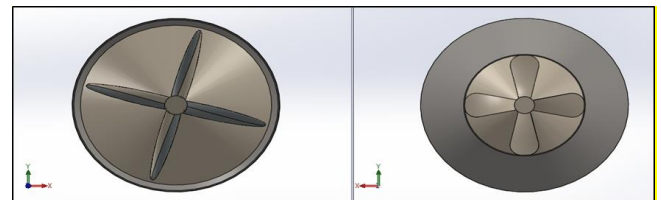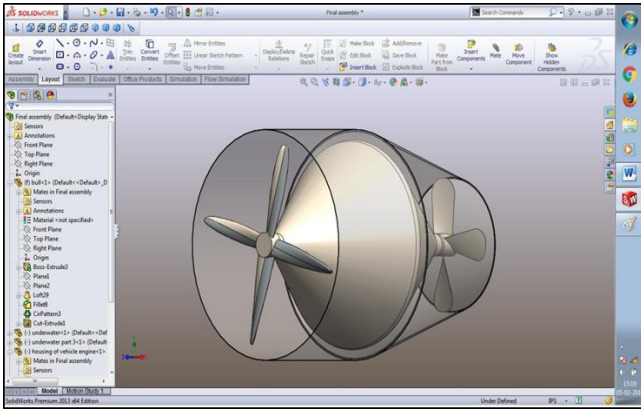

Figure 14. Two Views of Engine

Complete Propelling Engine View

A complete exploded view of the engine components and a transparent view of engine have been illustrated in **Figure 15, 16**.
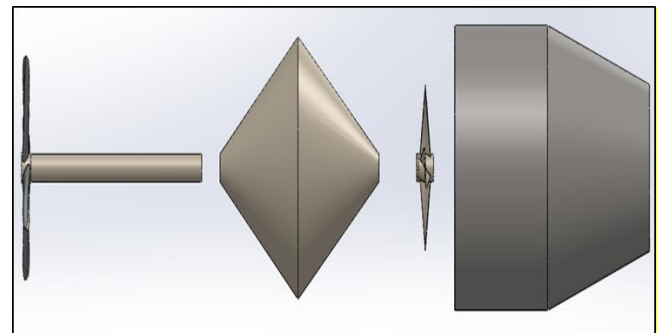
Figure 15. Exploded View of the Engine

Figure 16. Complete View of the Engine

EQUATIONS

The standard equations of Fluid Mechanics have been followed in devising the velocity of vehicle, drag coefficient, design of the engine and studying the characteristics of the flow through propeller at the inlet and turbine at the outlet. The terms used are in reference from **Table 1**.

a. $P = (\rho \times g \times q \times h)/1000$
b. $P = (2 * \pi * N * T)/60$
c. $V = \Phi\sqrt{(2 \times g \times h)}$
d. $\frac{P}{\rho g} + v * \frac{v}{2g} + z = \text{Constant}$
e. $\frac{m}{t} = \rho \times a \times V$
f. $u = \pi * D * N/60$
g. $a_1v_1 = a_2v_2 = a_3v_3 = av = \text{Constant}$
h. $f = (\text{Number of Poles}) * \frac{N}{120}$
i. $\partial u/ \partial t + u \cdot \nabla u = g - 1/ \rho \nabla p + \nu\nabla 2u$
j. $\partial u /\partial t + u \cdot \nabla u = g - 1/ \rho \nabla p$

Calculations

Design calculations such as Pressure Ratio, Electric Engine Specification, Clearance, Angle of Attack, Propeller Blade, Turbine Blade, Compressive Body and Mechanical Component specifications have been thoroughly devised so as to enable a proper design of engine considering all criteria of design failures.

Pressure Ratio

Pressure ratio acts as an integral part of increasing velocity across a component during its running condition. Higher the pressure ratios, more is the pressure developed across and therefore higher velocity is achieved. The pressure ratios are depicted in **Table 2**.

Table 2. Pressure Ratio achieved across components

Component	Pressure Ratio
Across Propeller	1.64
Across Compressor	3.4

Electric Engine Specifications

The standard specifications and ratings of electrical components are derived on the basis of design calculations and the desired output. The battery sizing and motor was selected on the basis of the maximum running time period of the engine. If the battery is operating at 375 Voltage**,** the alternator has to run at 25 voltages more than the battery voltage so as to allow recharging. The alternator simultaneously will recharge the battery with a charge rate current of 90.32 A. This would take 4.25 hours to recharge the battery completely at 20% efficiency loss. **Table 3** depicts the specification of electric engine.

Table 3. Electrical Engine Component Specifications

Specifications	Value
Weight of the Motor	50 Kg
Power Delivered by Motor	270 KW
Power to Weight Ratio	5.4
Battery Sizing	
Battery Energy	75 KWh
Battery Pack Voltage	375 V
Each Battery Voltage	3.78 V
Battery Capacity	320 Ah
Ampere per cell	10 A
Battery Weight	540 Kg
Length of each Battery	70 mm
Diameter of each Battery	21 mm
Range of Battery	400 to 420 km
Life-time of Battery	10 Years
Operating time of the Battery on a Single Take	32 Hours
Alternator	
Alternator Generating Voltage	400 V
Charge Rate Current	90.32 A/48 A
Alternator RPM	3600
Poles	2
Frequency	60 Hz
Phase	3
Current type	AC
Power Rating	2-50 KW
KVA	62.5
Power Factor	0.8
Cooling Type	Water Cooling
Charging Stations	
Super Charger (off-board)	120KW/DC
On-Board	50 KW/DC
Recharge Time (On-board)	4.25 Hours (100%)
Recharge Time (Off-Board)	1 Hour (100%)

Clearance Dimension

Clearance dimensions have been devised solely on the basis of design calculations and to cater hydraulic losses underwater that shall lead to the deterioration of the engine efficiency. The Bernoulli's theorem finds its use here. We know that reducing the area of flow increases the velocity of flow. The same principle is implemented here at each section such as the inlet, outlet and the clearance in between the top of the compressive body and the outer casing. By reducing the area of flow across the compressive body, the velocity is increased to almost three times to that of the inlet velocity. This increase in velocity is further increasing the velocity of the turbine at the outlet resulting in increase in efficiency and more power generation by the alternator. **Table 4** depicts the clearance space of the engine components with respect to the housing.

Table 4. Clearance with respect to the Engine Housing

Section	Clearance Diameter
Inlet	0.005 m
Mid-Section	0.34 m
Outlet	0.02 m

Optimization of Angle of Attack by Solidworks

The optimization is achieved in SolidWorks 2013 (Premium Version) by putting the assembled parts together. Flow simulation was performed by determining the velocity components, computational domain and specifying external flow over the assembly. Optimum angle of attack has been also observed and devised on the basis of the Aspect ratio as well as pressure ratio across the

components listed below to cater to the losses due to cavitation and drag force. Cavitation in simple terms is the formation of bubbles due to the fall of pressure below the vapour pressure of the liquid around. The bubbles formed during cavitation upon colliding with the blades result in intense shock and vibrations leading to decrease in efficiency and depletion in structural strength. Drag Force and pressure are inter-connected to each other. With decrease in pressure drag, the velocity increases due to which the pressure of the fluid flowing hardly falls below the vapour pressure of the fluid. The angle of attack therefore, has been devised on the objective of reducing the overall pressure drag and increase the maximum discharge through the engine. Maximum discharge here means, higher amount of water is being displaced by the propeller as well as the turbine to increase the velocity of vehicle in total. This is how, with increase in angle of attack, the process parameters are being optimized which are discussed in the table of mechanical specifications in details. Varying angles of attacks are depicted in **Table 5**.

Table 5. Taper or Twist Angle of the Mechanical Engine Components

Component	Section	Angle
Propeller Blade	Twist	3°
ompressive Body	Taper	20°
Turbine Blade	Twist	4°
Turbine Blade	Inlet	45.56°
Turbine Blade	Outlet	35°

Design of Propeller, Compressive Body and Turbine

The pitch as we know is the maximum amount of distance travelled by the propeller blade at the inlet during the flow. More the distance travelled by the propeller blade, more will be the discharge or more will be the amount of water entering into the engine through the inlet area. However, an average value of pitch was considered to increase the overall torque delivered. Too low the pitch, the torque output will reduce and too high propeller pitch will increase the wear and tear of the engine parts as well as reduce the acceleration of the vehicle by the engine.

The diameter of the engine components have been devised to cater to the compactness of the engine. Diameters of engine components are depicted in **table 6**.

Length of Engine – 1.87 m

Table 6. Diameter of Mechanical Engine Components

Engine Component	Diameter
Propeller Blade	0.28 m
Propeller Pitch	0.15 m
Inlet	0.565 m
Mid-Section	1.61 m
Outlet	0.62 m
Turbine	0.30 m

Mechanical Engine Specifications (Top Working Speed)

The mechanical engine specifications have been calculated by following the laws of hydraulics and hydrodynamics. The motor would be generating an rpm of 9000 rpm but due to increase in amount of

friction and density in water, the overall rpm delivered at the output is around 5990. This rpm will be transmitted to the shaft connecting the propeller at the inlet. The propeller with 6% slip at a total power use of 362 HP will enable in increasing the velocity of flow at the inlet from 2.5 m/sec to around 12 m/sec. This water will pass through the conduit past the compressive body with previously mentioned taper angle and clearance space which will result in a resultant velocity of around 32.12 m/sec. This high velocity water will hit the turbine blades which will in turn run the alternator at 2046 rpm. The alternator being connected to the battery will help in charging the battery simultaneously with a discharge of 20%. Higher the rpm, higher charge will be generated by the alternator. Upon successive CFD analysis with and without consideration of hydraulic losses, the velocity at the outlet will be 32.12 m/sec and 96.7 m/sec. Mechanical output is calculated and illustrated in **table 7**.
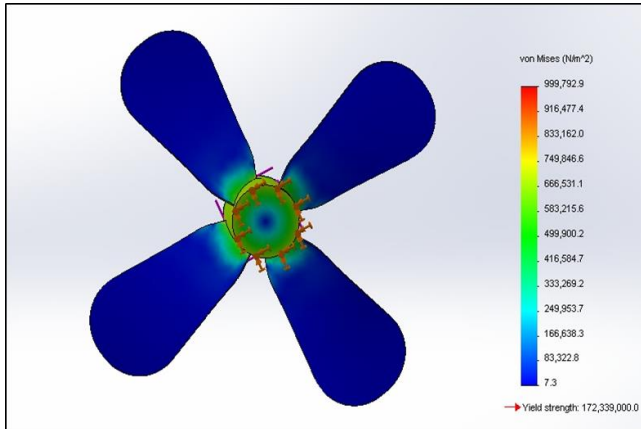
Stress and Flow Analysis

The flow analysis drop test and stress analysis has been demonstrated in **Figure 17-19** and performed on SolidWorks. The Stress Analysis was performed for the turbine blade which is subjected to a total Torque of 430.65 N-m. The results devised depicts that the material is well within the safety zone from fracture of the material where fracture due to stress at around 999,792.9 N/m^2 and failure due to torque at around 999.9 N-m. The results for turbine and propeller yielded the same results as the total torque would be same as they are connected co-axially to the same shaft. With the

flow analysis, it has been inferred that by neglecting all hydraulic losses, the highest velocity the engine can achieve is around 96.7 m/sec. However, taking consideration of vehicle weight, hydraulic losses and friction, the velocity attained by the vehicle shall be close to 60 m/sec.

Table 7. Mechanical Output

Specification	Value
Motor	
RPM	9000
Propeller	
Slip	6%
Propeller Gear Ratio	1:1
Power	362 HP
Velocity induced at inlet	11.63 m/sec
RPM	5990
Number of Blades	3
Compressive Body	
Velocity after Ram	32.12 m/sec
Turbine	
Speed Ratio	2.3
Head Delivered	10 m
Velocity at Turbine Blade (Inlet)	32.12 m/sec
Velocity at Turbine Blade (Outlet)	66.3 m/sec
RPM	2046
Number of Turbine Blade	4
Fluid	
Fluid Density	998.2 Kg/m^3
Flow Velocity of Sea Water	2.5 m/sec
Temperature	20 Degree Celsius
Overall Outlet	
Velocity	32.12 m/sec

Figure 17. Stress Analysis of Turbine Blade
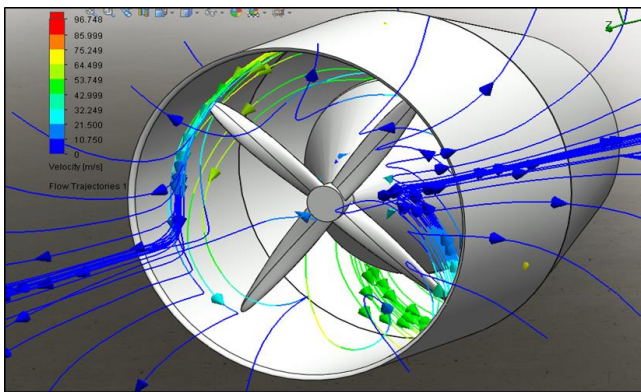
Figure 18. Flow Analysis of Engine
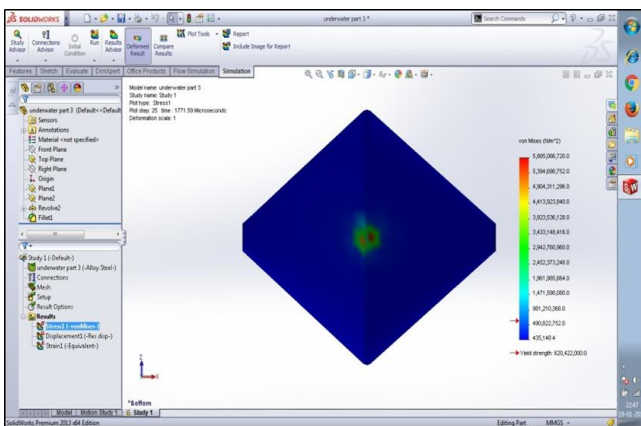
Figure 19. Fatigue Analysis of Compressive Body from a height of 100 m with reference to the plane

Table 8. Flow Simulation of Engine

LOAD ANALYSIS	
Calculated Torque	430.65 N-m
Maximum Torque before Failure	999.9 N-m
FLOW ANALYSIS	
Velocity of Vehicle (including all losses and friction)	32.12 m/sec
Velocity of Vehicle (excluding all losses and friction)	96.7 m/sec
STRESS ANALYSIS	
Stress at which failure occurs	999.672 KN/m^2

CONCLUSION

The present situation of resources depleting calls for an innovation that will eradicate the dependence of transport running on fuel. The purpose of the research is to address this problem and to suggest a no-fuel consuming electric vehicle that will efficiently serve short range operations ranging from 300 to 400 Km. The short range applications can be many, for example, it can be used as a military vehicle, can be used as an underwater environment friendly commercial transport, can be used as an alternative to clear off sea wastes in a short amount of time and can serve a crucial role in the cold chain industry by reducing the time gap between storage of food products and distribution in market thereby reducing post-harvest losses. Furthermore, the design provides an increase in performance in contrast to that of the submarine engine.

REFERENCES

1. Affanni, A., Bellini, A., Franceschini, G., Guglielmi, P., & Tassoni, C. (2005). Battery choice and management for new-generation electric vehicles. IEEE Transactions on Industrial Electronics, 52(5), 1343-1349.

2. Berckmans, G., Messagie, M., Smekens, J., Omar, N., Vanhaverbeke, L., & Van Mierlo, J. (2017). Cost projection of state of the art lithium-ion batteries for electric vehicles up to 2030. Energies, 10(9), 1314.

3. Bontempo, R., & Manna, M. (2018). Performance analysis of ducted marine propellers. part ii–accelerating duct. Applied Ocean Research, 75, 153-164.

4. Caccia, M., & Veruggio, G. (2000). Guidance and control of a reconfigurable unmanned underwater vehicle. Control engineering practice, 8(1), 21-37.

5. Chau, K. T., Chan, C. C., & Liu, C. (2008). Overview of permanent-magnet brushless drives for electric and hybrid electric vehicles. IEEE Transactions on industrial electronics, 55(6), 2246-2257.

6. Cristi, R., Papoulias, F. A., & Healey, A. J. (1990). Adaptive sliding mode control of autonomous underwater vehicles in the dive plane. IEEE journal of Oceanic Engineering, 15(3), 152-160.

7. Field, A.I., Cherchas, D., & Calisal, S. (2000). Optimal control of an autonomous underwater vehicle. World Automatic Congress, Hawaii, USA.

8. Fossen, T. I., & Sagatun, S. I. (1991). Adaptive control of nonlinear systems: A case study of underwater robotic systems. Journal of Robotic Systems, 8(3), 393-412.

9. Fossen, T. I. (1994). Guidance and control of ocean vehicles. John Wiley & Sons Inc.

10. Healey, A. J., & Marco, D. B. (1992, January). Slow speed flight control of autonomous underwater vehicles: Experimental results with NPS AUV II. In The Second International Offshore and Polar Engineering Conference. International Society of Offshore and Polar Engineers.

11. Herman, P. (2009). Decoupled PD set-point controller for underwater vehicles. Ocean Engineering, 36(6-7), 529-534.

12. Li, J. H., & Lee, P. M. (2005). Design of an adaptive nonlinear controller for depth control of an autonomous underwater vehicle. Ocean engineering, 32(17-18), 2165-2181.

13. Mahesh, H., Yuh, J., & Lakshmi, R. (1991). A coordinated control of an underwater vehicle and robotic manipulator. Journal of Robotic Systems, 8(3), 339-370.

14. Mcdonal, H., & Whitfield, D. (1997). Self-Propelled Maneuvering Underwater Vehicles. In National Research Council: Twenty-First Symposium on Naval Hydrodynamics. Washington, DC: The National Academies. 479-482.

15. Omar, N., Daowd, M., Bossche, P. V. D., Hegazy, O., Smekens, J., Coosemans, T., & Mierlo, J. V. (2012). Rechargeable energy storage systems for plug-in hybrid electric vehicles—Assessment of electrical characteristics. Energies, 5(8), 2952-2988.

16. Rodrigues, L., Tavares, P., & de Sousa Prado, M. G. (1996, September). Sliding mode control of an AUV in the diving and steering planes. In OCEANS 96 MTS/IEEE Conference Proceedings. The Coastal Ocean-Prospects for the 21st Century (Vol. 2, pp. 576-583). IEEE.

17. Shi, H., Gao, Z., Fan, Z., Ding, Y., Qiao, Y., & Zhu, Z. (2018). Corrosion Behavior of Alloy C-276 in Supercritical Water. Advances in Materials Science and Engineering, 2018.

18. Salgado-Jimenez, T., Spiewak, J. M., Fraisse, P., & Jouvencel, B. (2004, November). A robust control algorithm for AUV: based on a high order sliding mode. In Oceans' 04 MTS/IEEE Techno-Ocean'04 (IEEE Cat. No. 04CH37600) (Vol. 1, pp. 276-281). IEEE.

19. Soylu, S., Buckham, B. J., & Podhorodeski, R. P. (2008). A chattering-free sliding-mode controller for underwater vehicles with fault-tolerant infinity-norm thrust allocation. Ocean Engineering, 35(16), 1647-1659.

20. Xin, X., & Chengning, Z. (2017). Optimal Design of Electric Vehicle Power System with the Principle of Minimum Curb Mass. Energy Procedia, 105, 2629-2634.